# Tuning the viscoelastic response of hydrogel scaffolds with covalent and dynamic bonds

Drozdov, Aleksey D.; Christiansen, Jesper de Claville

*Published in:*
Journal of the Mechanical Behavior of Biomedical Materials

*DOI (link to publication from Publisher):*
10.1016/j.jmbbm.2022.105179



*Publication date:*
2022

*Document Version*
Publisher's PDF, also known as Version of record

journal of the mechanical behavior of biomedical materials 130 (2022) 105179

Contents lists available at ScienceDirect

Journal of the Mechanical Behavior of Biomedical Materials

journal homepage: www.elsevier.com/locate/jmbbm

Research paper

# Tuning the viscoelastic response of hydrogel scaffolds with covalent and dynamic bonds

Aleksey D. Drozdov *, Jesper deClaville Christiansen

*Department of Materials and Production Aalborg University Fibigerstraede 16, Aalborg 9220, Denmark*

ARTICLE INFO

*Keywords:*
Cell encapsulation
Supramolecular gel
Dynamic covalent gel
Viscoelasticity
Modeling

ABSTRACT

The processes of growth, proliferation and differentiation of stem cells encapsulated in 3D hydrogel microenvironments are strongly affected by the viscoelastic properties of the platforms. As the viscoelastic response of a hydrogel is determined by the rates of thermally induced dissociation of reversible cross-links, its modulation by introduction of several types of supramolecular and/or dynamic covalent bonds with different characteristic lifetimes has recently become a hot topic.

To reduce the number of experiments needed for design of hydrogel microenvironments with required mechanical properties, a model is developed for the viscoelastic and viscoplastic responses of hydrogels with multiple networks bridged by covalent and physical bonds. An advantage of the model is that it (i) involves a small number of material parameters, (ii) describes observations in rheological and mechanical tests in a unified manner, and (iii) predicts conventional measures of viscoelasticity used in the analysis of viability of cells.

## 1. Introduction

Growth and differentiation of stem cells in 3D microenvironments are regulated by a number of stimuli, which include (i) soluble factors (growth factors and cytokines), (ii) matrix-mediated signals (governed by the applied stresses, as well as the topography and stiffness of the platforms for cell culture), and (iii) cell–cell communication (Guilak et al., 2009; Kshitiz Park et al., 2012). The influence of elastic properties of the microenvironments on the regulation of cell behavior has attracted substantial attention in the past two decades (Lv et al., 2015; Vining and Mooney, 2017; Janmey et al., 2020). It has recently been recognized that the fate and activity of stem cells are strongly affected by the viscoelastic (Cameron et al., 2014; Chaudhuri et al., 2015, 2016, 2020; Charrier et al., 2018) and viscoplastic (Yang et al., 2014; Nam et al., 2016; Grolma et al., 2020; Jia et al., 2021) responses of their microenvironments. This discovery has led to a shift of the research focus on (i) regulation of the cellular functions by the dissipative properties of 3D platforms for cell culture (Dey et al., 2019; Cantini et al., 2020; Elosegui-Artola, 2021) and (ii) design of hydrogels (used as artificial extracellular matrices) with tunable viscoelastic properties (Rosales and Anseth, 2016; Matellan and del Rio Hernandez, 2019; Ma et al., 2021; Tong et al., 2021).

Chemically cross-linked hydrogels (where polymer chains are merged in a network by covalent bonds) do not reveal a noticeable dissipation. To prepare gels with strong viscoelastic and viscoplastic responses, chains are to be connected by supramolecular and/or dynamic covalent bonds that rearrange (dissociate and re-associate) under deformation (Chaudhuri, 2017; Teng et al., 2019; Tang et al., 2021; Rizwan et al., 2021).

The viscoelastic properties of these gels are studied in relaxation and creep tests with strains in the range of linear viscoelasticity (below 0.2), small amplitude oscillatory tests, as well as tensile and compressive cyclic tests with moderate strains (in the range of 0.2 to 0.4) and various strain rates (Chaudhuri, 2017; Tang et al., 2021). Conventionally, several hydrogels with similar elastic moduli, but different rates of rearrangement of bonds are prepared. Afterwards, viability and spreading of cells in the cell-laden gels are investigated under static conditions. Finally, correlations are established between some measure of viscoelasticity of the hydrogel matrices and the degree of proliferation of cells.

The viscoelastic properties of gels are characterized by the following parameters: (i) the time $\tau_{\frac{1}{2}}$ necessary for the stress to reach a half of its maximum value in relaxation tests (Chaudhuri et al., 2016; Bauer et al., 2017; Lou et al., 2018), (ii) the loss tangent $\tan\delta$ or the loss modulus $G''$ measured at a fixed angular frequency $\omega$ in oscillatory tests (Richardson et al., 2019, 2020, 2021; Mundhara et al., 2021; Nguyen et al., 2021), and (iii) the dissipative energy $D$ (the area under the stress–strain curve in uniaxial tensile test with a fixed strain rate) (Sacco et al., 2020).

* Corresponding author.
*E-mail address:* aleksey@m-tech.aau.dk (A.D. Drozdov).

https://doi.org/10.1016/j.jmbbm.2022.105179
Received 18 July 2021; Received in revised form 9 November 2021; Accepted 12 March 2022
Available online 26 March 2022

Observations show higher degrees of viability and larger spreading areas of cells cultured in hydrogel matrices with stronger viscoelastic properties (characterized by lower values of $\tau_{\frac{1}{2}}$, $D$ and higher values of $\tan\delta$ and $G''$).

To ensure high degrees of viability and proliferation of cells, the characteristic relaxation times of hydrogels matrices for cell culture should be close to the characteristic cellular times (Wang and Heilshorn, 2015; Gong et al., 2018). To satisfy this condition, the viscoelastic response of these matrices (determined by the characteristic times for dissociation and re-association of reversible bond between chains) should be modulated.

Several methods for tuning the viscoelastic properties of hydrogels with reversible bonds were recently discussed (Rosales and Anseth, 2016; Dey et al., 2019; Jing et al., 2021; Ma et al., 2021; Rizwan et al., 2021). They involve (Nam et al., 2019; Vining et al., 2019): (i) changes in concentration and molecular weight of polymer chain, (ii) regulation of concentration of physical bonds and addition of covalent cross-links, and (iii) alteration of the chain architecture (by grafting of short chains) and micro-structure of gels (due to hierarchical self-assembly of proteins).

A facile approach to tuning the viscoelastic response of hydrogels consists in replacement of some reversible bonds with the same amount of bonds with higher or lower rates of dissociation and re-association (Yesilyurt et al., 2017; Arkenberg et al., 2020; Xia et al., 2020). An advantage of this method is that does not induce changes in the elastic moduli of hydrogels (Teng et al., 2019; Rizwan et al., 2021). Richardson et al. (2019, 2020, 2021) applied this technique to poly(ethylene glycol) (PEG) gels cross-linked by dynamic covalent (alkyl-hydrazone and benzyl-hydrazone) bonds. Holten-Andersen et al. (2014) and Cazzell et al. (2021) used this method to modulate viscoelastic properties of end-functionalized PEG gels by changes in concentrations of divalent metal ions that form metal-ligand coordination bonds with catechol and histidine groups, respectively. Liu et al. (2017) demonstrated that replacement of a small amount of covalent bonds in the polyacrylamide gel with dynamic host-guest complexes based on cucurbit[8]uril resulted in a remarkable increase in energy dissipation and self-healing ability of these gels.

Design of hydrogels with supramolecular and dynamic covalent bonds to be used as 3D platforms for cell culture have recently become a hot topic (Jiang et al., 2019; Levalley and Kloxin, 2019; Ren et al., 2020; De Alwis Watuthanthrige et al., 2021). Despite substantial progress in this area, no simple approaches have been developed to predict parameters $\tau_{\frac{1}{2}}$, $\tan\delta$ and $D$ (conventionally used as measures of viscoelasticity for the microenvironments) for gels with several types of dynamic cross-links when these quantities are known for each type of reversible bonds separately.

The objective of this study is threefold:

1. To derive a simple model with a small number of material constants able to describe observations in shear relaxation tests, creep tests and small-amplitude oscillatory tests, as well as uniaxial tensile, compressive and cyclic tests with moderate strains on hydrogels with permanent and temporary bonds.
2. To extend the model for prediction of the viscoelastoplastic response of hydrogels whose chains are cross-linked by two families of reversible bonds with different rates of dissociation and re-association.
3. To analyze numerically the viscoelastic behavior of a gel whose polymer network consists of two sub-networks with similar elastic moduli, but different kinetics of rearrangement of bonds, and to evaluate how the measures of viscoelasticity $\tau_{\frac{1}{2}}$, $\tan\delta$ and $D$ of the double-network gel are affected by concentration $R$ of the second network.

Development of constitutive models for the elastic, viscoelastic and viscoplastic responses of double-network gels with supramolecular and dynamic covalent cross-links has attracted noticeable attention in the past decade (Liu et al., 2016; Mao et al., 2017; Drozdov and deClavill Christiansen, 2018a,b; Lu et al., 2018; Yu et al., 2018; Khiem et al., 2019; Lin et al., 2020; Javadi et al., 2021; Xiao et al., 2021), see also reviews (Guo and Long, 2020; Xiang et al., 2020; Lei et al., 2021). Unlike previous studies, we focus on derivation of constitutive equations with the minimum number of material parameters. This allows correlations to be established between the experimental measures of viscoelasticity $\tau_{\frac{1}{2}}$, $\tan\delta$ and $D$ in the physiological interval of frequencies and strain rates (Mao et al., 2021).

The exposition is organized as follows. A model for the viscoelastoplastic response of a hydrogel with covalent and physical cross-links is presented in Section 2. A detailed derivation of the governing equations is provided in Supplementary Material. In Section 3, the model is applied to describe observations in rheological (shear relaxation, creep and oscillatory tests with small strains) and mechanical (tensile, compressive and cyclic tests with large deformations) tests on gels with various types of dynamic bonds, and correlations are discussed between the measures of viscoelasticity $\tau_{\frac{1}{2}}$, $\tan\delta$ and $D$. In Section 4, constitutive equations for the mechanical behavior of a double-network gel with different kinetics of rearrangement of sub-networks are reported, and the effect of concentration of the secondary network on the viscoelastic response of the gel is studied numerically. Concluding remarks are formulated in Section 5.

## 2. Constitutive model

A gel is modeled as a two-phase medium consisting of a network of polymer chains and water molecules. The network is composed of two sub-networks: permanent and transient. Chains in the transient network are connected by dynamic bonds whose rearrangement (dissociation and re-association) is driven by thermal fluctuations. Chains in the permanent network are bridged by covalent cross-links and physical bonds whose characteristic time for rearrangement exceeds strongly the characteristic time for deformation. Focusing on the analysis of "rapid" loadings (whose rate is substantially higher than the rate of water diffusion), we disregard transport of water molecules through the gel.

To simplify the analysis, the neo-Hookean expression is accepted for the mechanical energy of a polymer chain. This relation was derived within the concept of entropic elasticity in Drozdov (2014). More sophisticated formulas for the strain energy density of the polymer network were developed and verified by comparison with observations under multi-axial deformation in Drozdov and Christiansen (2013, 2018).

With reference to Filippidi et al. (2017), the viscoplastic response of a gel is modeled as sliding of junctions between chains with respect to their reference positions. A junction starts to slide when one of the chains connected by this junction is transformed from the active state into the dangling state (and stresses in this chain vanish suddenly). Sliding proceeds until the junction reaches a new equilibrium state. The viscoplastic flow of junctions between chains is described by the associative law

$$\mathbf{D}_{\rm p} = \mathcal{P}\boldsymbol{\Sigma}', \tag{1}$$

where $\mathbf{D}_{\rm p}$ is the rate-of-strain tensor for plastic deformation, $\boldsymbol{\Sigma}'$ is the deviatoric component of the Cauchy stress tensor $\boldsymbol{\Sigma}$, and $\mathcal{P}$ is a scalar function. A more sophisticated model for viscoplastic flow with two mechanisms of sliding of junctions was developed in Drozdov et al. (2013).

According to the concept of transient networks (Green and Tobolsky, 1946; Tanaka and Edwards, 1992), the viscoelastic response of a gel reflects breakage and reformation (dissociation and re-association) of temporary bonds between chains. The gel is thought of as an inhomogeneous medium consisting of meso-domains with various activation energies $u$ for rearrangement (Drozdov, 1997). For a reversible bond

belonging to a meso-domain with a dimensionless activation energy $\upsilon = u/(k_B T)$, where $T$ stands for the absolute temperature, and $k_B$ denotes the Boltzmann constant, the rate of thermally induced breakage is determined by the Eyring formula

$$\Gamma(\upsilon) = \Gamma_0 \exp(-\upsilon), \tag{2}$$

where the pre-factor $\Gamma_0$ may, in general, be affected by external factors (degree of swelling, intensity of applied stresses, etc.).

The non-homogeneity of the network is characterized by the probability density $f(\upsilon)$ to find a meso-region with activation energy $\upsilon \geq 0$. With reference to the random energy model (Derrida, 1980), this function is described by the quasi-Gaussian formula,

$$f(\upsilon) = f_0 \exp\Big(-\frac{\upsilon^2}{2\Sigma^2}\Big), \tag{3}$$

where the coefficient $f_0$ is found from the normalization condition

$$\int_0^\infty f(\upsilon) \mathrm{d}\upsilon = 1. \tag{4}$$

Constitutive equations for the viscoelastoplastic response of a gel with covalent and physical cross-links under an arbitrary three-dimensional deformation with finite strains are developed in Supplementary Material.

Under uniaxial tension of a gel with a constant strain rate $\dot{\epsilon}$, the engineering tensile stress $\sigma$ is determined by the equations

$$\sigma = \frac{G}{\lambda}\Big[(1-\kappa)\Big(\lambda_e^2 - \frac{1}{\lambda_e}\Big) + \kappa \int_0^\infty f(\upsilon)\Big(S_1 \lambda_e^2 - \frac{S_2}{\lambda_e}\Big)\mathrm{d}\upsilon\Big], \tag{5}$$

where

$$\lambda = 1 + \dot{\epsilon} t \tag{6}$$

stands for the elongation ratio for macro-deformation. The elongation ratio for elastic deformation $\lambda_e$ obeys the differential equation

$$\frac{\dot{\lambda}_e}{\lambda_e} = \frac{\dot{\lambda}}{\lambda} - \frac{2}{3}\mathcal{P}\lambda\sigma, \qquad \lambda_e(0) = 1, \tag{7}$$

where the superscript dot stands for the derivative with respect to time $t$. The functions $S_1(t,\upsilon)$ and $S_2(t,\upsilon)$ in Eq. (5) are governed by the equations

$$\dot{S}_1 = \Gamma(\upsilon)(\lambda_e^{-2} - S_1), \qquad \dot{S}_2 = \Gamma(\upsilon)(\lambda_e - S_2), \qquad S_1(0,\upsilon) = S_2(0,\upsilon) = 1. \tag{8}$$

Eqs. (5)–(8) with the function $\mathcal{P}$ in the form

$$\mathcal{P} = P_1 \exp(-a\sigma) \quad \text{(loading)}, \qquad \mathcal{P} = P_2 \exp(-a\sigma) \quad \text{(unloading)} \tag{9}$$

describe tension ($\dot{\epsilon} > 0$), compression ($\dot{\epsilon} < 0$) and cyclic deformation (loading–retraction) of hydrogels in the unified manner. These relations differ from the governing equations in viscoelastoplasticity of hydrogels (Drozdov and deClavill Christiansen, 2018a,b) based on another approach to modeling the viscoplastic flow of junctions.

In a shear relaxation test with a small strain $\epsilon_0$ and the loading program

$$\epsilon(t) = 0 \quad (t < 0), \qquad \epsilon(t) = \epsilon_0 \quad (t \geq 0), \tag{10}$$

the decay in stress with time is determined by the formula

$$\sigma(t) = G\epsilon_0\Big[(1-\kappa) + \kappa \int_0^\infty f(\upsilon)\exp\Big(-\Gamma(\upsilon)t\Big)\mathrm{d}\upsilon\Big]. \tag{11}$$

In a shear creep test with a stress $\sigma_0$ and the loading program

$$\sigma(t) = 0 \quad (t < 0), \qquad \sigma(t) = \sigma_0 \quad (t \geq 0), \tag{12}$$

an increase in shear strain $\epsilon$ with time $t$ is governed by the equation

$$\epsilon(t) = \frac{\sigma_0}{G} + \kappa \int_0^\infty f(\upsilon) r(t,\upsilon)\mathrm{d}\upsilon, \tag{13}$$

where the function $r(t,\upsilon)$ obeys the differential equation

$$\dot{r} = \Gamma(\upsilon)(\epsilon - r), \qquad r(0,\upsilon) = 0. \tag{14}$$

For tensile and compressive relaxation tests, the shear modulus $G$ in Eqs. (11) and (13) is replaced with the Young's modulus. Keeping in mind the incompressibility condition (Eq. (S-1) in Supplementary Material), we write

$$E = 3G. \tag{15}$$

In a shear oscillatory test with a small amplitude $\epsilon_0$ and angular frequency $\omega$,

$$\epsilon(t) = \epsilon_0 \exp(\imath\omega t), \tag{16}$$

where $\imath = \sqrt{-1}$, the storage, $G'(\omega)$, and loss, $G''(\omega)$, moduli read

$$G'(\omega) = G\int_0^\infty f(\upsilon)\frac{(1-\kappa)\Gamma^2(\upsilon)+\omega^2}{\Gamma^2(\upsilon)+\omega^2}\mathrm{d}\upsilon,$$
$$G''(\omega) = G\int_0^\infty f(\upsilon)\frac{\kappa\Gamma(\upsilon)\omega}{\Gamma^2(\upsilon)+\omega^2}\mathrm{d}\upsilon. \tag{17}$$

where $\Gamma(\upsilon)$ is given by Eq. (2) with the pre-factor (Drozdov and deClavill Christiansen, 2021)

$$\Gamma_0 = \gamma(1 + K\omega). \tag{18}$$

Two advantages of Eqs. (2)–(18) are to be mentioned.

The model describes observations in cyclic tests under tension and compression, relaxation tests, creep tests and shear oscillatory tests in the unified manner. This allows the measures of the viscoelastic response of hydrogel platforms $\tau_{\frac{1}{2}}$, $\tan\delta$ and $D$ (determined in different tests) to be expressed in terms of each other.

The governing relations involve only eight material constants with transparent physical meaning: (i) $G$ stands for the shear modulus of a gel, (ii) $\kappa$ is the ratio of the number of temporary bonds to the total number of cross-links between chains, (iii) $\Sigma$ is a measure of inhomogeneity of the polymer network, (iv) $\gamma$ denotes the rate of thermally induced dissociation of dynamic bonds, (v) $K$ accounts for the influence of disentanglement and re-entanglement of chains on rearrangement of physical cross-links, (vi) $P_1$, $P_2$ and $a$ describe the viscoplastic flow of junctions between chains under loading and retraction.

## 3. Fitting of experimental data

Our aim now is to validate the ability of the model to describe (and to predict in some cases) experimental data on hydrogels with covalent and dynamic bonds subjected to various deformation programs.

### 3.1. Gels with physical bonds

To demonstrate that the model with the same material constants describes adequately observations in relaxation tests, creep tests and oscillatory tests simultaneously, we analyze two sets of experimental data on multi-arm PEG gels whose chains are bridged by dynamic covalent cross-links and supramolecular bonds.

#### 3.1.1. PEG gels with alkyl-hydrazone and benzyl-hydrazone bonds

We begin with matching experimental data on PEG gels cross-linked by alkyl-hydrazone (AH) and benzyl-hydrazone (BH) dynamic covalent bonds (Richardson et al., 2019, 2020, 2021). The chemical structure of the gels and their preparation conditions are described in Supplementary Material.

Observations in shear relaxation tests at temperature $T = 37$ °C (Richardson et al., 2019) on PEG gels with various concentrations of AH bonds $\phi$ are depicted in Fig. 1A, where the normalized shear stress $\bar{\sigma}(t) = \sigma(t)/\sigma(0)$ is plotted versus relaxation time $t$. Each set of data is fitted separately by means of Eqs. (2), (3) and (11) with three adjustable parameters ($\kappa$, $\gamma$ and $\Sigma$). Keeping in mind that all bonds between chains are temporary, we set $\kappa = 1$. The remaining two coefficients, $\gamma$ and $\Sigma$, are determined by the nonlinear regression method to minimize the expression

$$\sum\Big(\bar{\sigma}_{exp} - \bar{\sigma}_{sim}\Big)^2,$$

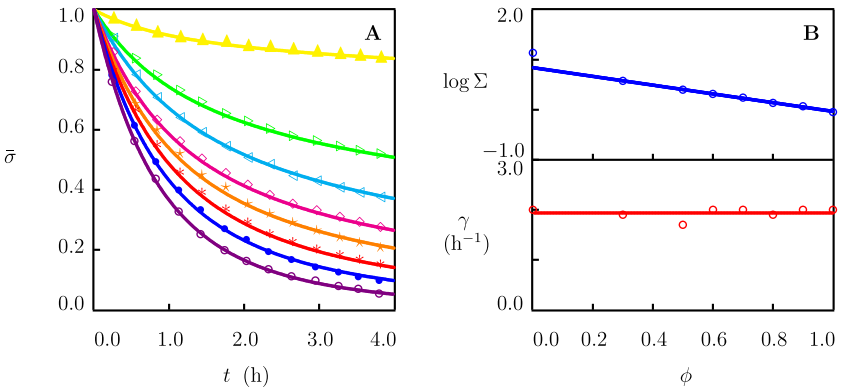


**Fig. 1.** A — Normalized shear stress $\bar{\sigma}$ versus relaxation time $t$. Symbols: experimental data (Richardson et al., 2019) on multi-arm PEG gels cross-linked with AH and BH bonds at temperature $T = 37$ °C. (Concentration of AH bonds: ▲ – $\phi = 0.0$, ▷ – $\phi = 0.3$, ◁ – $\phi = 0.5$, ◇ – $\phi = 0.6$, ★ – $\phi = 0.7$, ∗ – $\phi = 0.8$, • – $\phi = 0.9$, ○ – $\phi = 1.0$). Solid lines: results of simulation. B — Parameters $\Sigma$ and $\gamma$ versus $\phi$. Circles: treatment of observations. Solid lines: results of simulation.

where $\bar{\sigma}_{\rm exp}$ is the normalized stress measured in the test, $\bar{\sigma}_{\rm sim}$ stands for the prediction of Eq. (11), and summation is performed over all times $t$ at which observations are presented.

The effect of concentration of AH bonds on the material parameters is illustrated in Fig. 1B, where $\Sigma$ and $\gamma$ are plotted versus $\phi$. The data are approximated by the phenomenological relations

$$\log \Sigma = \Sigma_0 - \Sigma_1 \phi, \qquad \gamma = \gamma_0, \tag{19}$$

where $\log = \log_{10}$, and the coefficients in Eq. (19) are calculated by the least-squares technique. Fig. 1B shows that the measure of inhomogeneity of the polymer network $\Sigma$ decreases exponentially with concentration of AH bonds, whereas the rate of dissociation of bonds $\gamma$ remains independent of $\phi$.

Experimental data in shear relaxation tests at temperature $T = 25$ °C (Richardson et al., 2020) on PEG gels with concentrations of AH bonds $\phi = 0.78$ and 1.0 are reported in Figs. 2A and 2B. Observations (Richardson et al., 2020) in shear creep tests with stress $\sigma_0 = 100$ Pa at the same temperature are presented in Fig. 2C and 2D, where tensile strain $\epsilon$ is depicted versus creep time $t$. Each set of data in Figs. 2A and 2B is fitted separately by means of two adjustable parameters ($\gamma$ and $\Sigma$). Afterwards, the coefficient $\Sigma$ is fixed, and the data in Figs. 2C and 2D are approximated with the help of the model (2), (3), (13) and (14). The shear modulus $G$ is found from Eq. (13) at $t = 0$. The coefficient $\gamma$ is determined by the nonlinear regression method to minimize the expression

$$\sum \Big(\epsilon_{\rm exp} - \epsilon_{\rm sim}\Big)^2,$$

where summation is conducted over all experimental points.

Fig. 2 demonstrates good agreement between the observations in relaxation and creep tests and the results of simulation with the material parameters collected in Tab. S-1 (Supplementary Material). This table shows some discrepancies (by 33% at $\phi = 0.78$ and by 6% at $\phi = 1.0$) between the rates of dissociation of dynamic bonds $\gamma$ calculated by matching observations in relaxation and creep tests. These deviations may be explained by inaccuracies in measurements.

Experimental data (Richardson et al., 2021) in shear relaxation test with strain $\epsilon_0 = 0.1$, creep test with stress $\sigma_0 = 100$ Pa, and oscillatory test with strain amplitude $\epsilon_0 = 0.01$ on PEG gel with concentration of AH bonds $\phi = 0.39$ at temperature $T = 25$ °C are reported in Fig. 3 together with results of simulation with the material constants listed in Tab. S-2. We begin with fitting observations in relaxation test. Material parameters $\gamma$ and $\Sigma$ are found from the best-fit condition for the data depicted in Fig. 3A. After fixing these quantities, the elastic modulus $G$ is determined by matching the experimental creep curve in Fig. 3B. The coefficients $G$ and $K$ are determined separately by fitting the data in oscillatory tests (Fig. 3C) with the help of Eqs. (2), (3), (17) and (18). These quantities are found by the nonlinear regression method to minimize the expression

$$\sum_{\omega} \Big[\Big(G'_{\rm exp}(\omega) - G'_{\rm sim}(\omega)\Big)^2 + \Big(G''_{\rm exp}(\omega) - G''_{\rm sim}(\omega)\Big)^2\Big],$$

where $G'_{\rm exp}(\omega)$ and $G''_{\rm exp}(\omega)$ are the storage and loss moduli measured in a test, $G'_{\rm sim}(\omega)$ and $G''_{\rm sim}(\omega)$ are results of simulation, and summation is performed over all frequencies $\omega$ for which observations are provided.

Fig. 3 shows an acceptable agreement between the experimental data and results of simulation. Tab. S-2 demonstrates that the shear moduli calculated by fitting observations in the creep test and the oscillatory test adopt similar values (their difference does not exceed 18%). It follows from Tabs. S-1 and S-2 that the rate of dissociation of bonds $\gamma$ at temperature $T = 25$ °C is practically independent of $\phi$ (this quantity equals 1.4, 1.35 and 1.5 h$^{-1}$ at $\phi = 0.39$, 0.78 and 1.0, respectively). This conclusion is in accord with the results obtained at temperature $T = 37$ °C and plotted in Fig. 1B. Although the theoretical concentration of dynamic bonds in the polymer network remains constant, observations show that their real concentration (proportional to the shear modulus $G$) decreases noticeably with the growth of concentration $\phi$ of AH bonds. According to Tabs. S-1 and S-2, the shear modulus $G$ decays from 7.87 ($\phi = 0.39$) to 0.66 ($\phi = 0.66$) to 0.31 ($\phi = 1.0$) kPa.

### 3.1.2. PEG gels cross-linked with $Fe^{3+}$ ions and $Fe_3O_4$ nanoparticles

To examine the ability of the model to predict observations, we study experimental data in shear oscillatory tests and shear relaxation tests on catechol-functionalized tetra-arm PEG gel cross-linked by metal-ligand coordination bonds with $Fe^{3+}$ ions (Li et al., 2016). The chemical composition of the gel, the preparation procedure and the experimental conditions are described in Supplementary Material.

Experimental data in shear oscillatory test are presented in Fig. 4 A together with results of simulation with the material constants reported in Tab. S-3. Using these parameters, the response of the gel in shear relaxation test is predicted by means of Eqs. (2), (3) and (11). Results of simulation are compared with observations in Fig. 4B. This figure demonstrates an acceptable agreement between predictions of the model and experimental data. Small deviations along the initial stage of relaxation (when relaxation time $t$ remains below 1 s) are driven by the time-dependent response along the loading path which is not accounted for in Eq. (10).

To compare the viscoelastic behavior of catechol-functionalized PEG gel cross-linked with $Fe^{3+}$ ions with that of the PEG gel cross-linked by metal-ligand coordination bonds at the surfaces of $Fe_3O_4$ nanoparticles, we fit the experimental data in Fig. 5 (Li et al., 2016). The preparation conditions for the nanocomposite gel and the experimental procedure are described in Supplementary Material.

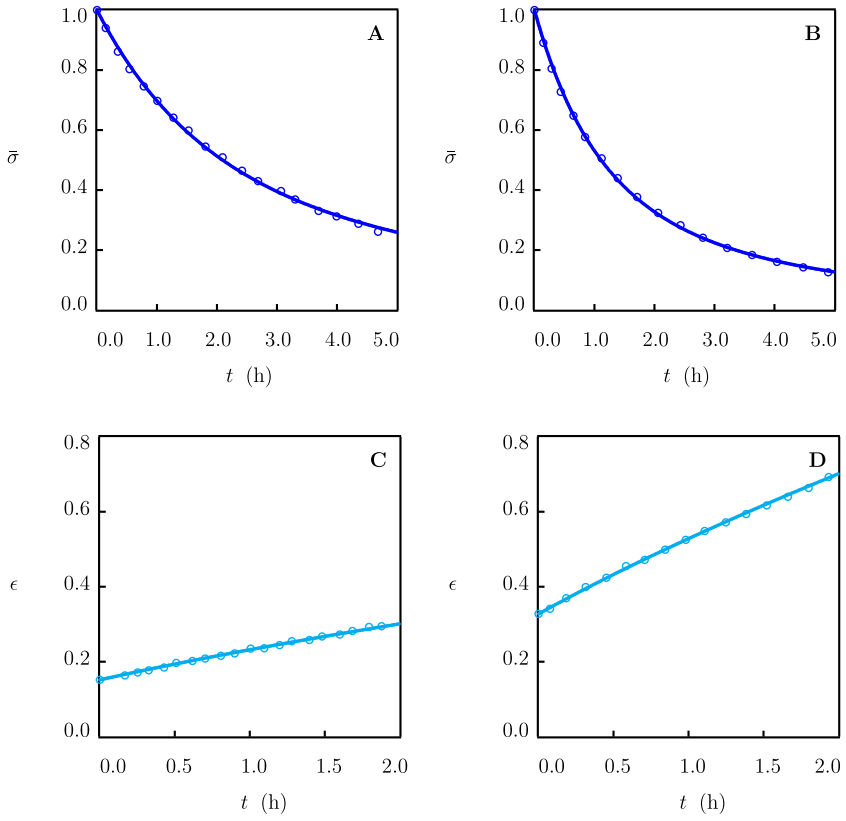


**Fig. 2.** A, B — Normalized shear stress $\bar{\sigma}$ versus relaxation time $t$. C, D — Shear strain $\epsilon$ versus creep time $t$. Circles: experimental data (Richardson et al., 2020) on PEG gels cross-linked with AH and BH bonds at temperature $T = 25$ °C. The concentrations of AH bonds equal $\phi = 0.78$ (A, C) and $\phi = 1.0$ (B,D). Solid lines: results of simulation.

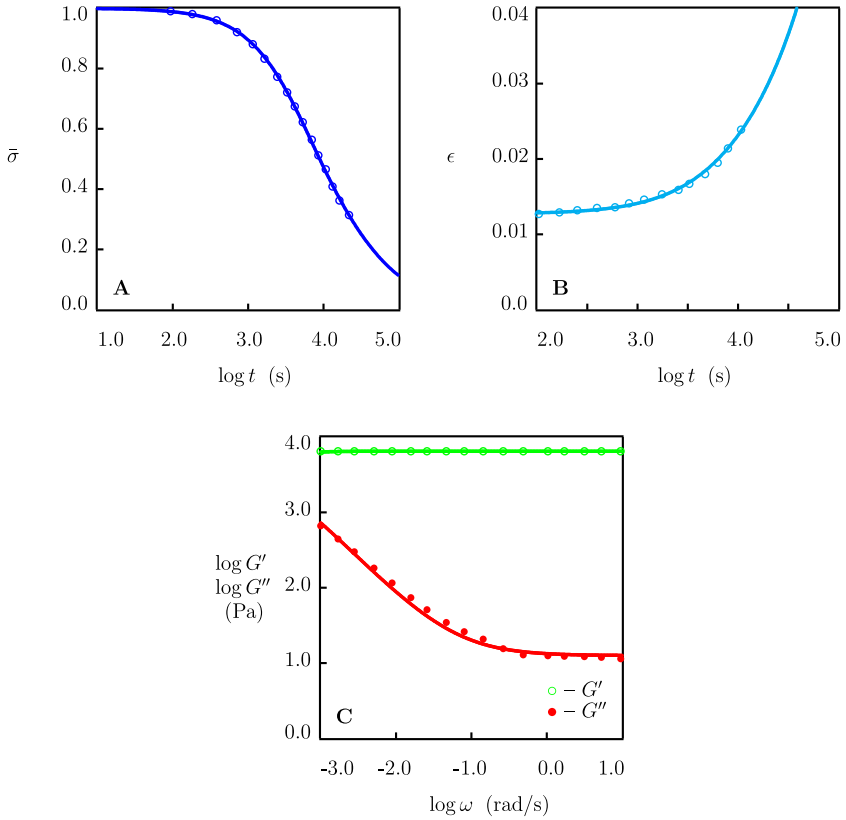


**Fig. 3.** A — Normalized shear stress $\bar{\sigma}$ versus relaxation time $t$. B — Shear strain $\epsilon$ versus creep time $t$. C — Storage modulus $G'$ and loss modulus $G''$ versus frequency $\omega$. Symbols: experimental data (Richardson et al., 2021) at temperature $T = 25$ °C on PEG gel cross-linked with AH and BH bonds with concentration of AH bonds $\phi = 0.39$. Solid lines: results of simulation.

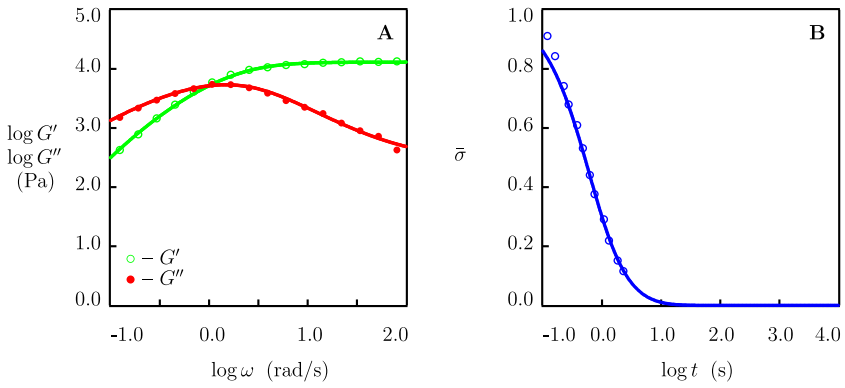


**Fig. 4.** A — Storage modulus $G'$ and loss modulus $G''$ versus frequency $\omega$. B — Normalized shear stress $\bar{\sigma}$ versus relaxation time $t$. Symbols: experimental data (Li et al., 2016) on catechol-functionalized PEG gel cross-linked with $Fe^{3+}$ ions in a buffer solution with pH = 12 at temperature $T = 20$ °C. Solid lines: results of simulation (A) and predictions of the model (B).

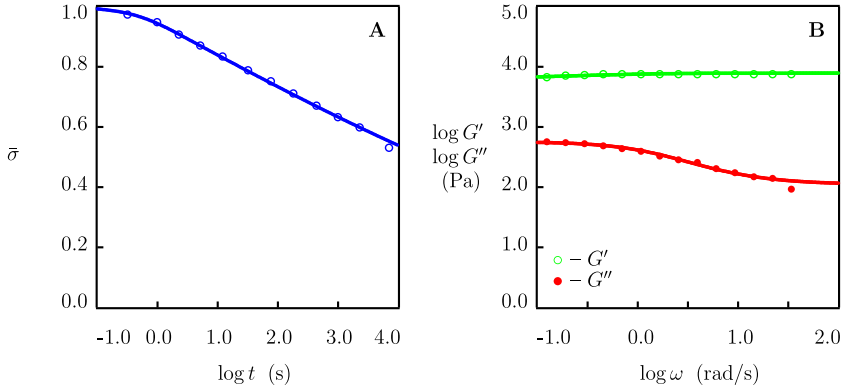


**Fig. 5.** A — Normalized shear stress $\bar{\sigma}$ versus relaxation time $t$. B — Storage modulus $G'$ and loss modulus $G''$ versus frequency $\omega$. Symbols: experimental data (Li et al., 2016) on catechol-functionalized PEG gel cross-linked with $Fe_3O_4$ nanoparticles. Solid lines: results of simulation.

The coefficients $\gamma$, $\Sigma$ and $\kappa$ are found by matching observations in shear relaxation test (Fig. 5A). Then, these quantities are fixed, and observations in shear oscillatory test (Fig. 5B) are fitted by means of two coefficients, $G$ and $K$. Fig. 5 demonstrates that both sets of data are described adequately by the model with the material parameters reported in Tab. S-3.

According to Tab. S-3, replacement of $Fe^{3+}$ ions with iron oxide nanoparticles as a cross-linker induces (i) a decay (approximately by twice) in the shear modulus $G$ of the gel and the rate of dissociation of dynamic bonds $\gamma$ and (ii) a pronounced (by an order of magnitude) increase in the measure of inhomogeneity of the network $\Sigma$ and the coefficient $K$ that accounts for the effect of disentanglement of chains on rearrangement of physical bonds. These changes may be explained by a strong increase in disorder of the polymer network when chains are cross-linked by large (compared with $Fe^{3+}$ cations) nanoparticles.

### 3.2. Gels with permanent and physical cross-links

To examine how the presence of permanent cross-links in the polymer network affects the viscoelastic response of gels with physical bonds, two sets of experimental data are analyzed.

#### 3.2.1. Recombinant protein gels

We begin with fitting observations on two recombinant protein gels (Yang et al., 2018). The gels (designated as AXA+BXB and AXA+BBB) were prepared by mixing solutions of two proteins with elastin-like polypeptides (AXA and BXB, AXA and BBB, respectively). It is presumed (Yang et al., 2018) that chains in the gels are bridged by permanent isopeptide SpyTag–SpyCatcher cross-links and temporary bonds between entangled dimers of the proteins. The chemical structure of the proteins, the preparation procedure for the gels, and the experimental conditions are described in Supplementary Material.

Experimental data in shear relaxation tests and shear oscillatory tests at room temperature are presented in Figs. 6A, 6B (AXA+BXB) and 6C, 6D (AXA+BBB), respectively. For each gel, we begin with fitting observations in relaxation tests by means of three adjustable parameters ($\gamma$, $\Sigma$ and $\kappa$). Afterwards, these quantities are fixed, and observations in oscillatory tests are matched with the help of two coefficients ($G$ and $K$).

Fig. 6 shows good agreement between the experimental data and results of simulation with the material constants collected in Tab. S-4. This table shows that the gel AXA+BXB contains physical cross-links only ($\kappa = 1$), whereas some chains in the gel AXA+BBB are bridged by covalent cross-links ($\kappa = 0.84$). The presence of permanent bonds in the protein gel results in a weak increase in the shear modulus $G$ (by 10%) and the measure of inhomogeneity of the network $\Sigma$ (by 23%), and it does not affect the rate of dissociation of dynamic bonds $\gamma$ and the coefficient $K$.

#### 3.2.2. HA gels with single and double networks

We analyze experimental data in shear oscillatory tests at room temperature (Loebel et al., 2019) on two hyaluronic acid (HA) gels functionalized with 1-adamantane acetic acid (Ad) and 6-(6-aminohexyl) amino-6-deoxy-$\beta$-cyclodextrin (CD) and cross-linked by supramolecular adamantane-cyclodextrin host-guest (HG) complexes. Preparation of the gels and experimental conditions are described in Supplementary Material.

Observations on the gels with mass fractions of HA $\phi = 0.03$ and 0.05 are reported in Figs. 7A and 7B, respectively, together with results

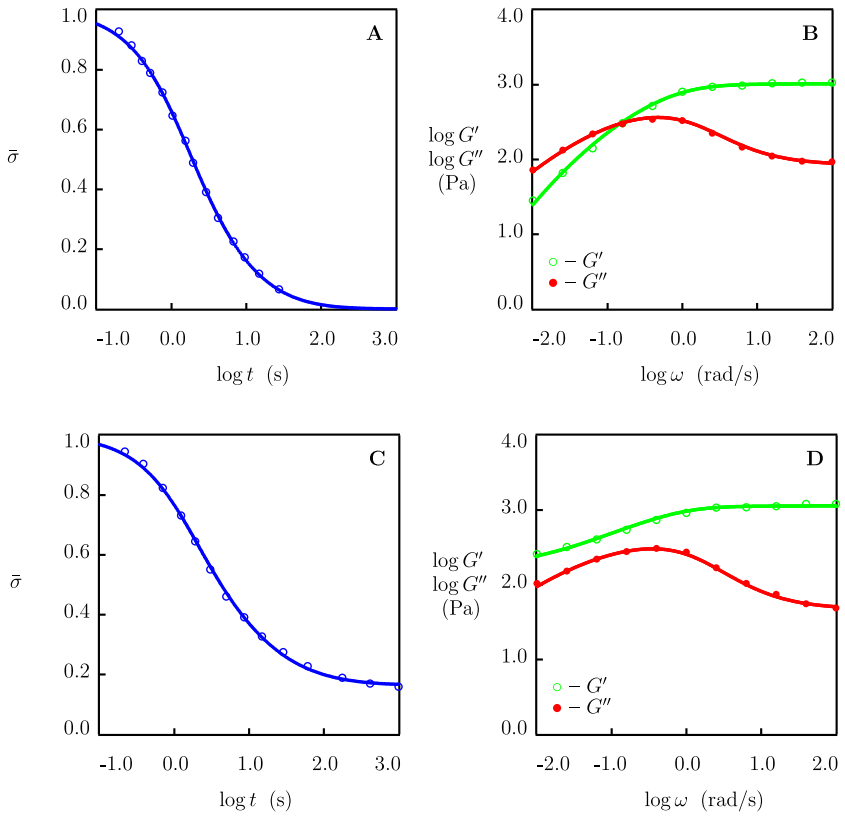


**Fig. 6.** A, C — Normalized shear stress $\bar{\sigma}$ versus relaxation time $t$. B, D — Storage modulus $G'$ and loss modulus $G''$ versus frequency $\omega$. Symbols: experimental data (Yang et al., 2018) at room temperature on recombinant protein gels cross-linked by SpyTag–SpyCatcher and isopeptide bonds (A,B – AXA+BXB, C,D – AXA+BBB). Solid lines: results of simulation.

of simulation with the material constants listed in Tab. S-5. This table shows that the growth of mass fraction of HA $\phi$ induces a strong (by a factor of 4) increase in the shear modulus $G$, a weak (by 11%) reduction in the measure of inhomogeneity $\Sigma$, and does not affect the parameters $\gamma$, $\kappa$ and $K$.

For comparison, observations (Loebel et al., 2019) are fitted on two double-network gels, in which the first network is formed by HA chains bridged by host-guest complexes (mass fractions of polymer $\phi = 0.03$ and 0.05), and the other network is formed by linear PEG chains end-functionalized with bovine fibrinogen and diacrylate and covalently cross-linked by fibrinogen–diacrylate bonds (mass fractions of PEG-fibrinogen and PEG-diacrylate chains equal 0.0085 and 0.02). Details of the preparation procedure are provided in Supplementary Material.

Experimental data in shear oscillatory tests on these gels are depicted in Fig. 7C and 7D (for $\phi = 0.03$ and 0.05, respectively), together with results of numerical analysis with the material constants collected in Tab. S-5.

Figs. 7A to 7D reveal that the presence of the network with covalent bonds results in substantial (by several orders of magnitude) growth in the storage and loss moduli at low angular frequencies $\omega$ (below 1 rad/s). Although this effect is reduced with frequency $\omega$, $G'$ and $G''$ of the double-network gels exceed their counterparts of the single-network gels by several times even at $\omega = 10^3$ rad/s. According to Tab. S-5, these changes are driven by an increase in the shear modulus of the network $G$, a noticeable growth of the measure of its inhomogeneity $\Sigma$, and a pronounced slowing down of the rearrangement process for supramolecular bonds (characterized by the coefficient $\gamma$).

### 3.3. Observations in rheological and mechanical tests

To evaluate the ability of the model (with the same material parameters) to describe experimental data in rheological (small-amplitude shear oscillations) and mechanical (tensile, compressive and cyclic) tests simultaneously, three sets of observations are analyzed.

#### 3.3.1. HA gels with single and double networks

Single-network HA gel (with concentration of HA $\phi = 0.05$) cross-linked by host-guest interactions between Ad and CD units was synthesized (Rodell et al., 2016) by using the same procedure as the gel (Loebel et al., 2019) whose response is illustrated in Fig. 7B.

Observations in shear oscillatory test at temperature $T = 37$ °C (Rodell et al., 2016) are reported in Fig. 8A together with results of simulation with the material parameters listed in Tab. S-6. Comparison of Tabs. S-5 and S-6 shows that the coefficients $\kappa$, $\gamma$ and $K$ adopt similar values, whereas the shear modulus $G$ and the parameter $\Sigma$ in Tab. S-6 are lower (by 46% and 23%, respectively) than the same coefficients in Tab. S-5. The latter may be explained by different temperatures at which the tests were conducted.

Methacrylated HA (MeHA) was synthesized by esterification of HA with methacrylic anhydride (MA). Double-network HA gel (with physical cross-links formed by Ad-CD complexes and covalent cross-links between methacrylates and thiols) was prepared by mixing solutions of functionalized HA chains (HA-Ad and HA-CD, concentration 0.05) and MeHA chains (concentration 0.03) in the presence of dithiothreitol (DTT). The chemical composition of the gel and its preparation procedure are described in Supplementary Material.

Experimental data in uniaxial tensile and compressive tests on the double-network gel are presented in Figs. 8B and 8C, where the engineering stress $\sigma$ is plotted versus tensile and compressive strain $\epsilon$, respectively. As observations in rheological tests on this gel were not provided, the data in Figs. 8B and 8C are approximated by means of the model (2), (3), (5), (7)–(9) with the coefficients $G$ and $\gamma$ found by matching the experimental dependencies in Fig. 8A. We disregard the viscoplastic flow of junctions between chains by setting $P_1 = 0$ in Eq. (9) and fit each set of data separately with the help of two parameters ($\Sigma$ and $\kappa$). Their best-fit values are determined from the condition of minimum for the expression

$$\sum \left( \sigma_{\rm exp} - \sigma_{\rm sim} \right)^2,$$

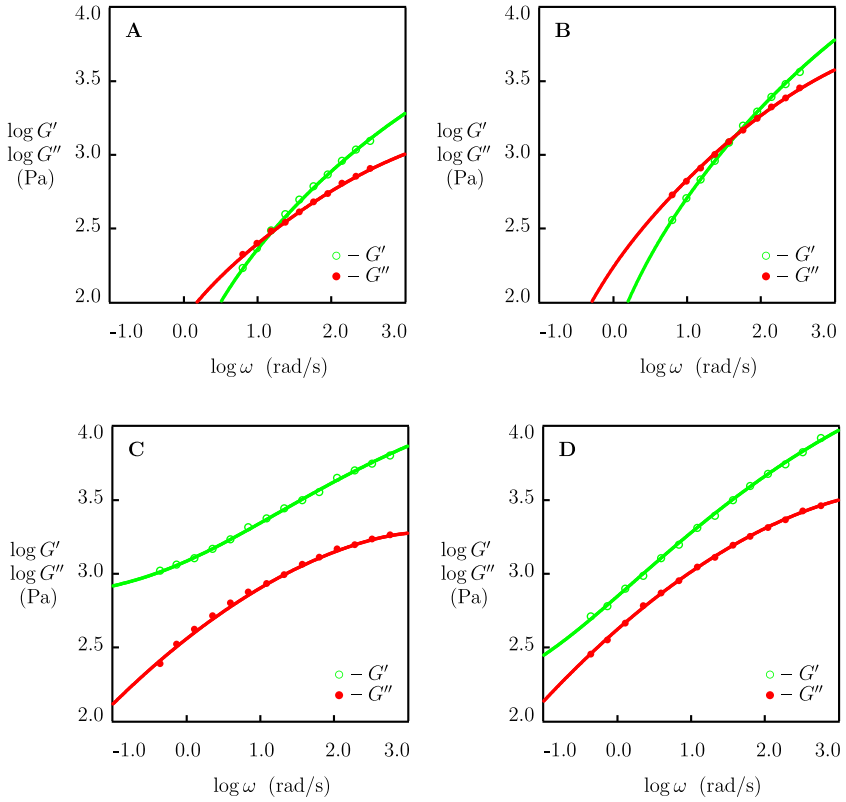


**Fig. 7.** Storage modulus $G'$ and loss modulus $G''$ versus frequency $\omega$. Symbols: experimental data (Loebel et al., 2019) on HA gels at room temperature. Solid lines: results of simulation. A, B — single-network HA gels (mass fractions of HA equal 0.03 (A) and 0.05 (B)) cross-linked by Ad-CD host-guest interactions. C, D — double-network gels with HA supramolecular network and PEG covalently cross-linked network (mass fraction of PEG equals 0.0285, mass fractions of HA equal 0.03 (C) and 0.05 (D)).

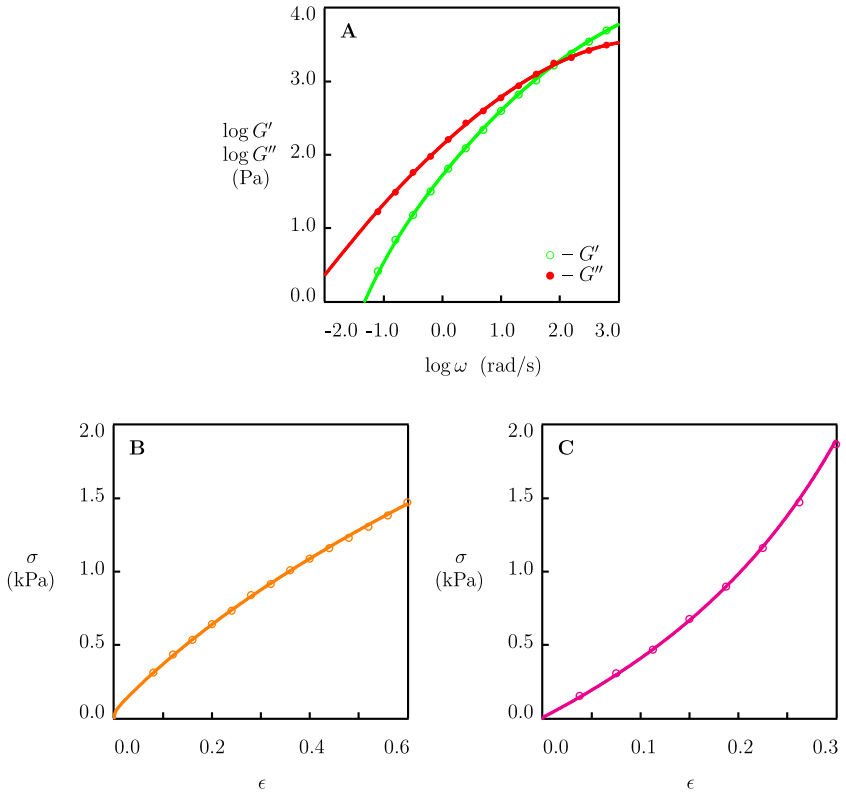


**Fig. 8.** A — Storage modulus $G'$ and loss modulus $G''$ versus frequency $\omega$. Symbols: experimental data (Rodell et al., 2016) on single-network HA gel cross-linked by Ad-CD host-guest interactions at temperature $T = 37$ °C. Solid lines: results of simulation. B, C — Tensile stress $\sigma$ versus tensile strain $\epsilon$ (B) and compressive stress $\sigma$ versus compressive strain $\epsilon$ (C). Circles: experimental data (Rodell et al., 2016) on double-network HA gel with covalent cross-links and dynamic Ad-CD bonds at room temperature. Solid lines: results of simulation.

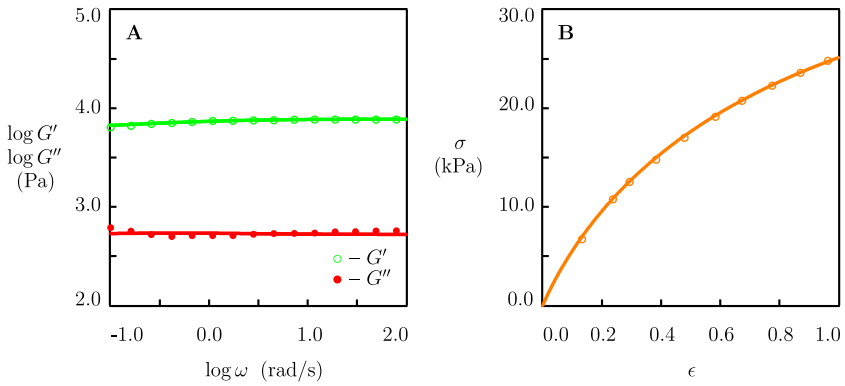


**Fig. 9.** A — Storage modulus $G'$ and loss modulus $G''$ versus frequency $\omega$. B — Tensile stress $\sigma$ versus tensile strain $\epsilon$. Symbols: experimental data (Zhao et al., 2020) on BSA gel cross-linked by BSA-glutaraldehyde bonds at room temperature. Solid lines: results of simulation.

where $\sigma_{exp}$ is the stress measured in a test, $\sigma_{sim}$ stands for the prediction of Eq. (5), and summation is performed over all strains $\epsilon$ at which observations are reported. Figs. 8B and 8C demonstrate good agreement between the experimental data in tensile and compressive tests and results of simulation with the material constants collected in Tab. S-6. According to this table, formation of the secondary network with chains cross-linked by covalent bonds induces a (rather weak) decay in the coefficient $\kappa$ (that characterizes concentration of dynamic bonds between chains) and a strong (by 42%) reduction in the measure of inhomogeneity of the network $\Sigma$. Although observations in tensile and compressive tests are matched separately, the best-fit values of $\kappa$ and $\Sigma$ found in their approximation coincide practically.

### 3.3.2. BSA gel cross-linked by BSA-glutaraldehyde bonds

Bovine serum albumin (BSA) gel with the Michael-type BSA-glutaraldehyde bonds was synthesized (Zhao et al., 2020) by mixing aqueous solutions of BSA and glutaraldehyde. The preparation procedure for the protein gel and the experimental conditions are given in Supplementary Material.

Observations on this gel in shear oscillatory test and uniaxial tensile test at room temperature are reported in Fig. 9 together with results of simulation with the material constants listed in Tab. S-7. We set $\kappa = 1$ and find the coefficients $G$, $\gamma$, $\Sigma$ and $K$ by matching the experimental data in Fig. 9A. After fixing these parameters, the data in tensile test (Fig. 9B) are fitted by means of two coefficients ($P_1$ and $a$).

### 3.3.3. Triple cross-linked P(AAm-AAc-UPy) copolymer gel

Poly(acrylamide–acrylic acid–2-ureido-4-pyrimidone) P(AAm-AAc-UPy) copolymer gel was prepared (Liu et al., 2020) by free radical polymerization of a solution AAm, AAc and UPyMA monomers in dimethyl sulfoxide. The organogel was immersed in an aqueous solution of $Fe^{3+}$ ions, and, finally, soaked in deionized water. The gel was cross-linked by hydrogen bonds between AAm and AAc segments, quadruple hydrogen bonds between UPyMA segments, and metal-coordination bonds between $Fe^{3+}$ ions and ionized carboxyl groups. Details of the preparation procedure and the experimental setup are reported in Supplementary Material.

Experimental data in small-amplitude shear oscillatory tests and uniaxial tensile loading–unloading tests at room temperature are depicted in Fig. 10 together with results of numerical analysis with the material constants collected in Tab. S-8. As repeatability of measurements in cyclic tests is rather low, two sets of data in cyclic tests (Figs. 5a and 5c in Liu et al. (2020) are approximated separately in Figs. 10B and 10C.

First, observations in the rheological test (Fig. 10A) are matched by the model with five adjustable parameters ($G$, $\gamma$, $\Sigma$, $\kappa$ and $K$). Afterwards, the quantities $\gamma$, $\Sigma$, $\kappa$ are fixed. To fit the stress–strain diagrams in cyclic tests, we set $P_1 = 0$ (no plastic flow under loading), and approximate each set of data with the help of three parameters ($G$, $P_2$ and $a$). Tab. S-8 demonstrates that the best-fit values of the shear modulus $G$ differ slightly (the maximal difference between their values does not exceed 25%), whereas the quantities $P_2$ and $a$ coincide practically for the observations depicted in Fig. 10B and 10C.

### 3.3.4. Double cross-linked catechol-functionalized PEG gels

Catechol-functionalized eight-arm PEG gels were synthesized by mixing catechol-terminated PEG chains and $Fe^{3+}$ ions (molar ratio of $Fe^{3+}$ and catechol 2:3) in aqueous solutions with pH = 3 at room temperature (Barrett et al., 2013). After preparation, the gels were equilibrated in buffer solutions with pH = 3, 5, 7, and 9. PEG gels were double cross-linked by covalent bonds between o-quinone groups (formed at pH = 3) and $Fe^{3+}$-catechol coordination complexes (developed under equilibration in solutions with pH = 5, 7 and 9). The preparation procedure and the experimental conditions are described in Supplementary Material.

Experimental data in compressive relaxation tests with strain $\epsilon_0 = 0.2$ are depicted in Fig. 11 together with results of simulation with the material constants collected in Tab. S-9. Each set of observations is matched separately with the help of four adjustable parameters ($E$, $\gamma$, $\Sigma$ and $\kappa$). Tab. S-9 shows that $\gamma$ and $\Sigma$ are weakly affected by pH, while $\kappa$ increases substantially with pH. The Young's modulus $E$ grows with pH under acidic conditions and reduces under alkaline conditions due to a decay in concentration of supramolecular bonds caused by formation of coordination complexes between $Fe^{3+}$ cations and mobile $OH^-$ anions, see (Holten-Andersen et al., 2011; Fullenkamp et al., 2014) for a discussion.

Observations in cyclic (loading–retraction) tests are reported in Fig. 12, where the engineering compressive stress $\sigma$ is plotted versus the engineering compressive strain $\epsilon$. Each set of data is matched separately by using the coefficients $E$, $\gamma$, $\Sigma$ and $\kappa$ reported in Tab. S-9. To reduce the number of adjustable parameters, we set $P_1 = 0$ and approximate each curve in Fig. 12 by means of only two parameters ($P_2$ and $a$). Their best-fit values are listed in Tab. S-9.

## 3.4. Discussion

Figs. 1 to 12 demonstrate good agreement between the experimental data in relaxation tests, creep tests, small-amplitude oscillatory tests, tensile tests and compressive tests and results of numerical analysis with the material parameters reported in Tabs. S-1 to S-9. It is shown that the model with eight material constants can describe (and to predict in some cases) the mechanical response of hydrogels whose chains are bridged by covalent cross-links and physical (supramolecular and dynamic covalent) bonds. Fig. 1 and Tabs. S-1 to S-9 reveal that material parameters evolve consistently with chemical composition and experimental conditions for the gels.

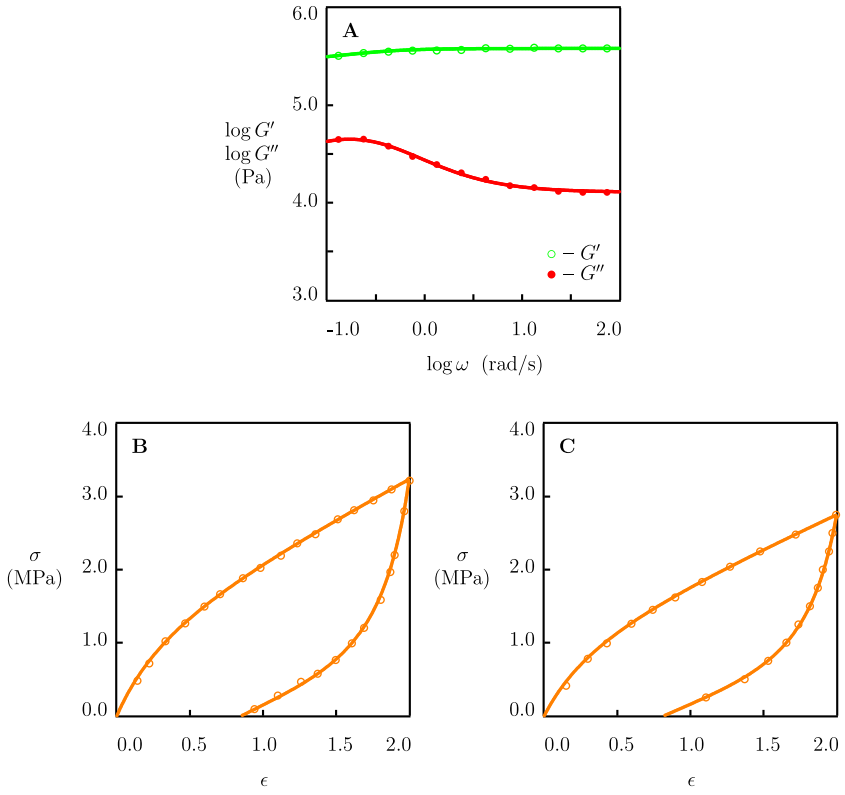


**Fig. 10.** A — Storage modulus $G'$ and loss modulus $G''$ versus frequency $\omega$. B, C — Tensile stress $\sigma$ versus tensile strain $\epsilon$. Symbols: experimental data (Liu et al., 2020) on triple cross-linked P(AAm-AAc-UPyMA) copolymer gel at temperature $T = 25$ °C. Solid lines: results of simulation.

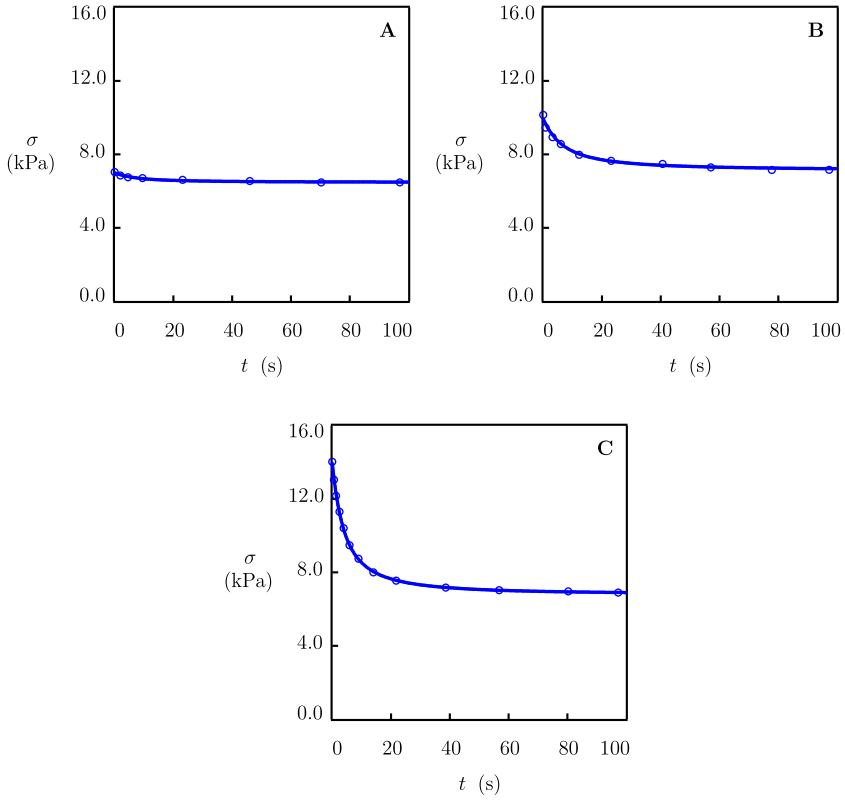


**Fig. 11.** Compressive stress $\sigma$ versus relaxation time $t$. Circles: experimental data (Barrett et al., 2013) in relaxation tests with strain $\epsilon_0 = 0.2$ on double cross-linked catechol-functionalized multi-arm PEG gels prepared in an aqueous solution of $Fe^{3+}$ ions with pH = 3 and equilibrated in buffers with various pH (A — pH = 5, B — pH = 7, C — pH = 9). Solid lines: results of simulation.

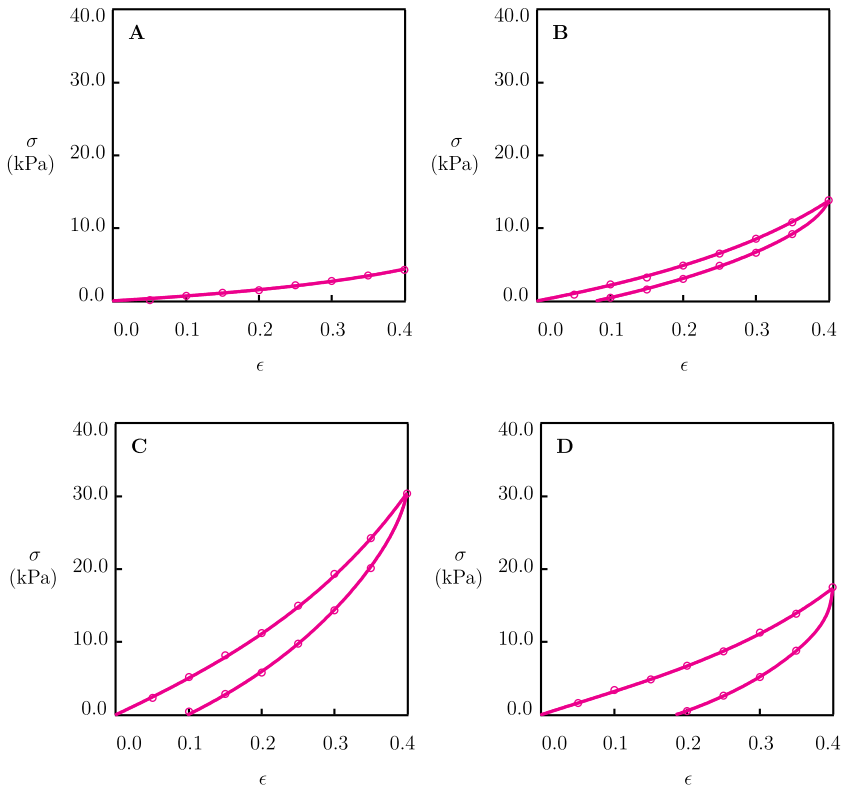


**Fig. 12.** Compressive stress $\sigma$ versus compressive strain $\epsilon$. Circles: experimental data (Barrett et al., 2013) in compressive cyclic tests on double cross-linked catechol-functionalized multi-arm PEG gels prepared in an aqueous solution of $Fe^{3+}$ ions with pH = 3 and equilibrated in buffers with various pH (A — pH = 3, B — pH = 5, C — pH = 7, D — pH = 9). Solid lines: results of simulation.

Three types of physical cross-links with various characteristic rates of dissociation are distinguished: (i) "slow" bonds with the rates of breakage of order of $10^{-4}$ to $10^{-3}$ $s^{-1}$ (alkyl-hydrazone and benzyl-hydrazone cross-links in Figs. 1 to 3), (ii) bonds with medium rates of rearrangement of order of $10^{-1}$ to 10 $s^{-1}$ ($Fe^{3+}$-catechol complexes in Figs. 4 and 11, $Fe^{3+}$-carboxyl complexes in Fig. 10, and protein gels in Figs. 6 and 9), and (iii) "rapid" bonds with the characteristic rates of breakage of order of $10^3$ to $10^4$ $s^{-1}$ (adamantane-cyclodextrin host-guest complexes in Figs. 7 and 8). Although the rate of dissociation of bonds $\gamma$ is not the only parameter that determines the relaxation rate (the measure of inhomogeneity of the network $\Sigma$ serves as the other parameter, see Figs. 4 and 5), this classification provides a clue which types of bonds are to be used in hydrogels with reversible bonds to modulate their viscoelastic properties.

Our aim now is to demonstrate that all three measures ($\tau_{\frac{1}{2}}$, $\tan\delta$ and $D$) used in the analysis of viability of cells encapsulated in hydrogel matrices can be tuned simultaneously by changing the type of bonds between chains without alteration of the elastic modulus. For this purpose, we analyze observations on collagen gels reported in Lui et al. (2020). The polymer network of the first hydrogel is formed (Liu et al., 2020) by covalently cross-linked collagen methacrylamide (C-MA) chains. The polymer network in the other gel is formed by collagen chains bridged by dynamic imine bonds (C-Ad) with linear PEG chains end-functionalized with dialdehyde. The composition of collagen gels, their preparation procedure and the experimental conditions are described in Supplementary Material.

Observations on C-MA and C-Ad gels in shear relaxation tests and small-amplitude oscillatory tests at room temperature are presented in Figs. S-1 and S-2, respectively, together with results of simulation with the material parameters collected in Tab. S-10. This table shows that the shear moduli $G$ and the rates of rearrangement of bonds $\gamma$ in the gels coincide practically. The viscoelastic response of the gels differ pronouncedly (see Figs. S-1A and S-2 A) due to the very low measure of inhomogeneity $\Sigma$ and a noticeably higher concentration of physical bonds $\kappa$ in C-Ad gel.

Presuming the coefficient $P_1$ to vanish (in accord with the results reported in Tabs. S-8 and S-9) and using the material parameters listed in Tab. S-10, we calculate the response of the collagen gels in relaxation tests with small strains, small-amplitude shear oscillatory tests, and tensile tests with strain rate $\dot{\epsilon} = 10$ $min^{-1}$ and maximum engineering strain $\epsilon_{max} = 0.6$.

Results of numerical analysis are presented in Fig. 13. This figure shows that replacement of covalent cross-links (C-MA) between chains with dynamic imine bonds (C-Ad) results in a pronounced (by a factor of 8) decrease in the relaxation time $\tau_{\frac{1}{2}}$, a strong increase in the loss tangent $\tan\delta$ (by a factor of 5 at $\omega = 1$ rad/s), and a substantial (by 70%) reduction in the coefficient $D$.

## 4. Tuning the viscoelastic response of hydrogels

A facile method of modulation of the viscoelastic response of a hydrogel with reversible cross-links (where chains in the network are bridged by a specific type of dynamic bonds characterized by the coefficients $\gamma^{(1)}$, $\Sigma^{(1)}$, $\kappa^{(1)}$ and $K^{(1)}$) consists in replacement of some transient bonds with orthogonal dynamic bonds (whose kinetics of dissociation is characterized by the coefficients $\gamma^{(2)}$, $\Sigma^{(2)}$, $\kappa^{(2)}$ and $K^{(2)}$). As a result, a double-network gel is formed whose polymer network involves two sub-networks with concentrations $\phi^{(1)} = 1 - R$ and $\phi^{(2)} = R$, where $R$ stands for the fraction of the second network (Picchioni and Muljana, 2018; Jiang et al., 2019; Hammer et al., 2021; De Alwis Watuthanthrige et al., 2021).

To determine concentrations $R$ that ensure the required viscoelastic properties of the double-network gel as a platform for cell encapsulation, correlations are to be established between the quantities $\tau_{\frac{1}{2}}$, $\tan\delta$ and $D$, on the one hand, and the coefficients $\gamma^{(m)}$, $\Sigma^{(m)}$, $\kappa^{(m)}$ and $K^{(m)}$

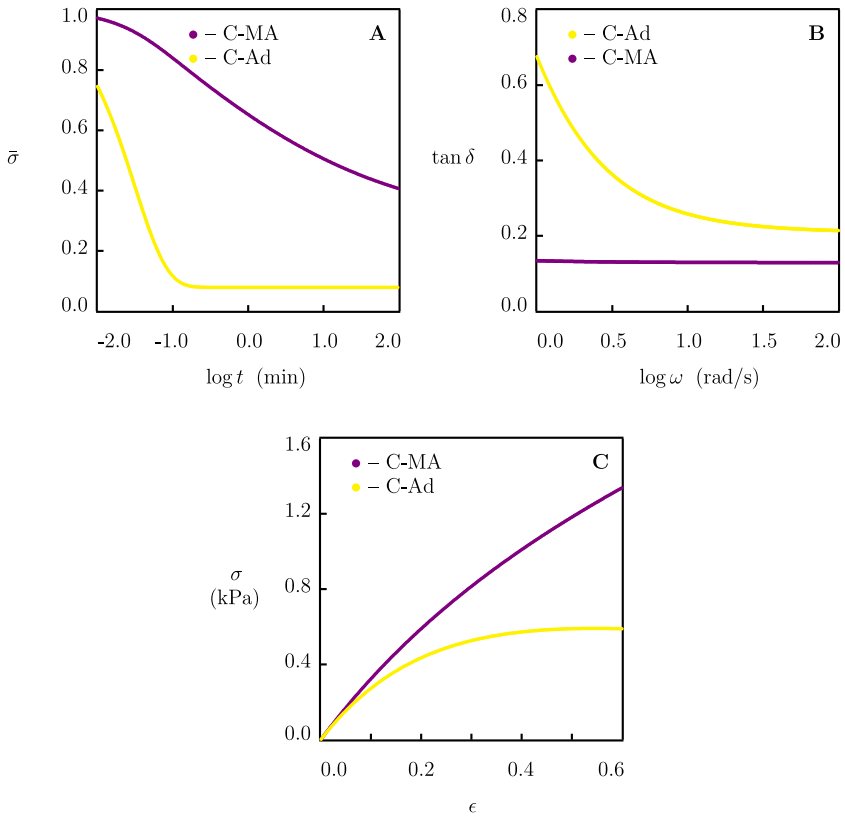


**Fig. 13.** A — Normalized stress $\bar{\sigma}$ versus relaxation time $t$. B — Tangent $\delta$ versus frequency $\omega$. C — Tensile stress $\sigma$ versus tensile strain $\epsilon$. Solid lines: results of simulation for covalently cross-linked (C-MA) and cross-linked by dynamic imine bonds (C-Ad) collagen gels.

$(m = 1, 2)$, on the other. For this purpose, interactions between the sub-networks are disregarded (as a first approximation) and the stress $\sigma$ in the network with two types of temporary bonds is calculated as the sum of stresses $\sigma^{(1)}$ and $\sigma^{(2)}$ in the corresponding sub-networks,

$$\sigma = \sigma^{(1)} + \sigma^{(2)}. \tag{20}$$

This approach implies that in a relaxation test with small strain $\epsilon_0$, the decay in the total stress $\sigma$ with relaxation time $t$ is determined by the analog of Eq. (11),

$$\sigma(t) = \epsilon_0 \sum_{m=1}^{2} G^{(m)} \phi^{(m)} \Big[ (1 - \kappa^{(m)}) + \kappa^{(m)} \int_0^{\infty} f^{(m)}(\upsilon) \exp\Big( -\gamma^{(m)} \exp(-\upsilon) t \Big) d\upsilon \Big], \tag{21}$$

where $G^{(m)}$ denotes the shear modulus of the $m$th network, and

$$f^{(m)}(\upsilon) = f_0^{(m)} \exp\Big( -\frac{\upsilon^2}{2(\Sigma^{(m)})^2} \Big). \tag{22}$$

The loss tangent $\tan\delta$ in a small-amplitude oscillatory test is given by

$$\tan\delta = \frac{G''}{G'}, \tag{23}$$

where the storage, $G'$, and loss, $G''$, moduli are found from the relations similar to Eq. (17),

$$G'(\omega) = \sum_{m=1}^{2} G^{(m)} \phi^{(m)} \int_0^{\infty} f^{(m)}(\upsilon) \frac{(1 - \kappa^{(m)})(\Gamma^{(m)}(\upsilon))^2 + \omega^2}{(\Gamma^{(m)}(\upsilon))^2 + \omega^2} d\upsilon,$$
$$G''(\omega) = \sum_{m=1}^{2} G^{(m)} \phi^{(m)} \int_0^{\infty} f^{(m)}(\upsilon) \frac{\kappa^{(m)} \Gamma^{(m)}(\upsilon) \omega}{(\Gamma^{(m)}(\upsilon))^2 + \omega^2} d\upsilon \tag{24}$$

with

$$\Gamma^{(m)}(\upsilon) = \gamma^{(m)}(1 + K^{(m)}\omega) \exp(-\upsilon). \tag{25}$$

The energy dissipated in uniaxial tensile test (6) with a constant strain rate $\dot{\epsilon}$ and a maximum strain $\epsilon_{\max}$ reads

$$D = \int_0^{\epsilon_{\max}} \sigma(t) \dot{\epsilon}\, dt, \tag{26}$$

where $\sigma$ is given Eq. (20), and $\sigma^{(m)}$ is determined by the analog of Eq. (5),

$$\sigma^{(m)} = \frac{G^{(m)} \phi^{(m)}}{\lambda} \Big[ 1 - \kappa^{(m)} \Big( (\lambda_e^{(m)})^2 - \frac{1}{\lambda_e^{(m)}} \Big)$$
$$+ \kappa^{(m)} \int_0^{\infty} f^{(m)}(\upsilon) \Big( S_1^{(m)} (\lambda_e^{(m)})^2 - \frac{S_2^{(m)}}{\lambda_e^{(m)}} \Big) d\upsilon \Big]. \tag{27}$$

It follows from Eqs. (7)–(9) that the elongation ratio for elastic deformation $\lambda_e^{(m)}$ and the functions $S_1^{(m)}$ and $S_2^{(m)}$ are governed by the equations

$$\frac{\dot{\lambda}_e^{(m)}}{\lambda_e^{(m)}} = \frac{\dot{\lambda}}{\lambda} - \frac{2}{3} P_1^{(m)} \sigma^{(m)} \exp\Big( -a^{(m)} \sigma^{(m)} \Big) \lambda, \qquad \lambda_e^{(m)}(0) = 1,$$
$$\dot{S}_1^{(m)} = \Gamma^{(m)} ((\lambda_e^{(m)})^{-2} - S_1^{(m)}), \qquad S_1^{(m)}(0, \upsilon) = 1,$$
$$\dot{S}_2^{(m)} = \Gamma^{(m)} (\lambda_e^{(m)} - S_2^{(m)}), \qquad S_2^{(m)}(0, \upsilon) = 1, \tag{28}$$

where the coefficients $P_1^{(m)}$ and $a^{(m)}$ characterize sliding of junctions between chains in the $m$th network.

To simplify the analysis, we disregard the influence of one family of bonds on the kinetics of rearrangement of the other family. A similar assumption was recently introduced and verified by Chen et al. (2021). This approach is approximate because (i) the rates of rearrangement can be affected by interactions between chains bridged by different types of bonds (Han et al., 2017; Tang et al., 2020), and (ii) these rates are mutually dependent when the bonds are formed due to multivalent interactions (Badjic et al., 2005; von Krbek et al., 2017; Weng and Wang, 2020).

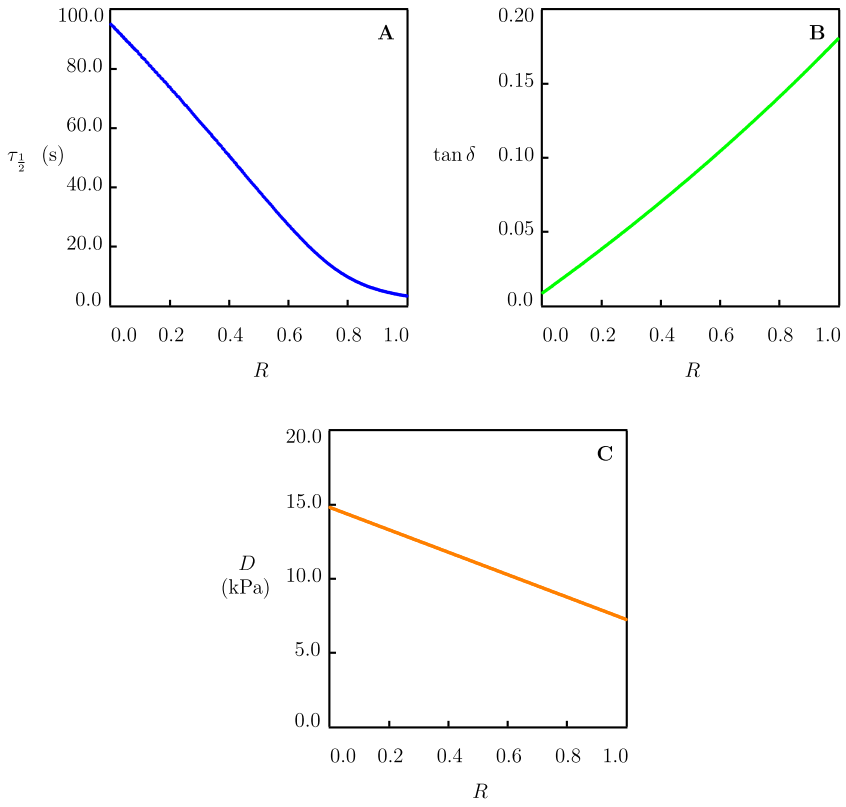


**Fig. 14.** The characteristic relaxation time $\tau_{\frac{1}{2}}$ (A), the loss tangent $\tan\delta$ (B) and the dissipated energy $D$ (C) versus concentration of the second network $R$. Solid lines: results of simulation for the double-network gel.

To examine the accuracy of our assumption, we apply Eq. (21) to predict the viscoelastic response in shear relaxation tests on PEG gels cross-linked by benzyl-hydrazone (BH, $m = 1$) and alkyl-hydrazone (AH, $m = 2$) bonds with various concentrations $R$ of AH bonds (Richardson et al., 2019). Simulation is conducted with $G^{(1)} = G^{(2)}$ and the material parameters $\gamma^{(m)}$ and $\Sigma^{(m)}$ reported in Fig. 1B. The experimental data and results of numerical analysis are depicted in Fig. S-3. This figure shows reasonable agreement between observations and predictions of the model at relatively small relaxation times (below 2 h). At higher durations of relaxation tests, the model underestimates slightly the amount of relaxed stress. For all relaxation times under consideration and all concentrations $R$ of AH bonds, the difference between the data and their predictions does not exceed 15%.

To evaluate changes in the quantities $\tau_{\frac{1}{2}}$, $\tan\delta$ and $D$ driven by an increase in concentration $R$ of the second network, numerical analysis is performed for a hypothetical double-network gel with the material constants collected in Tab. S-11. Both networks in the gel involve only dynamic bonds ($\kappa^{(1)} = \kappa^{(2)} = 1$), have similar shear moduli $G^{(m)}$, and do not reveal viscoplastic flow under tension ($P_1^{(1)} = P_1^{(2)} = 0$). The first network is homogeneous, but its rearrangement rate is low (small $\gamma^{(1)}$ and $\Sigma^{(1)}$), the other network is strongly inhomogeneous, but the rate of dissociation of bonds is relatively high (large $\gamma^{(2)}$ and $\Sigma^{(2)}$). Replacement of “slow" bonds in the first network with “rapid" bonds in the other network results in enhancement of the viscoelastic response.

This improvement is characterized in Fig. 14, where $\tau_{\frac{1}{2}}$, $\tan\delta$ and $D$ are plotted versus concentration $R$ of the second network ($\tan\delta$ is evaluated at frequency $f = 1$ Hz, dissipated energy $D$ is determined in tensile tests with strain rate $\dot{\epsilon} = 2$ min$^{-1}$ and maximum strain $\epsilon_{\max} = 0.6$). This figure provides quantitative predictions how the conventional measures of viscoelasticity of a hydrogel microenvironment for cell encapsulation can be tuned by changing concentrations of two families of reversible bonds.

## 5. Conclusions

A simple model is developed for the viscoelastic and viscoplastic responses of hydrogels with covalent and reversible cross-links. An advantage of the model is that describes adequately experimental data in rheological (shear relaxation, creep and small-amplitude oscillatory tests) and mechanical (tension, compression and cyclic loading with finite strains) experiments, on the one hand, and contains only eight material constants with transparent physical meaning (the minimum number needed to describe the elastic, viscoelastic and viscoplastic phenomena), on the other.

The list of material parameters involves: (i) the shear modulus $G$, (ii) the ratio of the number of reversible bonds to the total number of cross-links between chains $\kappa$, (iii) a measure of inhomogeneity of the polymer network $\Sigma$, (iv) the rate of dissociation of dynamic bonds $\gamma$, (v) a coefficient $K$ that accounts for the influence of disentanglement and re-entanglement of chains on rearrangement of physical bonds, (vi) the rates $P_1$, $P_2$ of sliding of junctions between chains under loading and retraction, and (vii) the coefficient $a$ characterizing the effect of stress on the viscoplastic flow.

The ability of the model to describe (and to predict in some cases) observations is confirmed by the analysis of experimental data on (i) poly(ethylene glycol) gels cross-linked by alkyl-hydrazone and benzyl-hydrazone dynamic covalent bonds, (ii) poly(ethylene glycol) gels cross-linked by supramolecular metal-ligand bonds with $Fe^{3+}$ ions and iron oxide nanoparticles, (iii) hyaluronic acid gels cross-linked by covalent cross-links and host-guest complexes between adamantane and cyclodextrin, (iv) triple cross-linked poly(acrylamide–acrylic acid–2-ureido-4-pyrimidone) copolymer gel, (v) recombinant protein gels cross-linked by permanent isopeptide bonds and reversible bonds between entangled proteins, and (vi) bovine serum albumin (BSA) gel cross-linked by the Michael-type BSA-glutaraldehyde bonds.

Three measures of viscoelasticity of hydrogel microenvironments are conventionally employed in the experimental analysis of viability of

cells: (i) the time $\tau_{\frac{1}{2}}$ necessary to reduce stress by twice in relaxation tests with small strains, (ii) the loss tangent $\tan\delta$ measured in small-amplitude oscillatory tests with a fixed frequency belonging to the physiological interval, and (iii) the energy $D$ dissipated under tension with fixed strain rate and maximum strain. The model established correlations between these quantities, which allows observations to be compared on different types of cells under different experimental conditions.

The governing equations are applied to predict these measures of viscoelasticity for single- and double-network gels with permanent and reversible cross-links. In particular, it is shown that replacement of covalent cross-links with dynamic imine bonds in a collagen gel results in a strong reduction in $\tau_{\frac{1}{2}}$ and $D$ and a noticeable increase in $\tan\delta$ simultaneously (Fig. 13). Evolution of the measures of viscoelasticity $\tau_{\frac{1}{2}}$, $\tan\delta$ and $D$ driven by replacement of "slow" bonds between chains with "rapid" bonds is studied numerically (Fig. 14). Although our approach to the analysis of the mechanical behavior of hydrogels with several types of reversible bonds is approximate (it disregards mutual interactions between the sub-networks), this methods can be used for "quick-and-dirty" predictions of the chemical structure of hydrogels with required viscoelastic properties.

## CRediT authorship contribution statement

**Aleksey D. Drozdov:** Conceptualization, Methodology, Software, Formal analysis, Writing–original draft, Writing – review & editing. **Jesper deClaville Christiansen:** Conceptualization, Methodology, Funding acquisition, writing – review & editing.

## Declaration of competing interest

The authors declare that they have no known competing financial interests or personal relationships that could have appeared to influence the work reported in this paper.

## Acknowledgments

Financial support by Innovationsfonden (Innovation Fund Denmark, project 9091-00010B) is gratefully acknowledged.

## Appendix A. Supplementary data

Supplementary material related to this article can be found online at https://doi.org/10.1016/j.jmbbm.2022.105179.

## References

Arkenberg, M.R., Nguyen, H.D., Lin, C.-C., 2020. Recent advances in bio-orthogonal and dynamic crosslinking of biomimetic hydrogels. J. Mater. Chem. B 8, 7835–7855.
Badjic, J.D., Nelson, A., Cantrill, S.J., Turnbull, W.B., Stoddart, J.F., 2005. Multivalency and cooperativity in supramolecular chemistry. Acc. Chem. Res. 38, 723–732.
Barrett, D.G., Fullenkamp, D.E., He, L., Holten-Andersen, N., Lee, K.Y.C., Messersmith, P.B., 2013. Ph-based regulation of hydrogel mechanical properties through mussel-inspired chemistry and processing. Adv. Funct. Mater. 23, 1111–1119.
Bauer, A., Gu, L., Kwee, B., Li, W.A., Dellacherie, M., Celiz, A.D., Mooney, D.J., 2017. Hydrogel substrate stress-relaxation regulates the spreading and proliferation of mouse myoblasts. Acta Biomater. 62, 82–90.
Cameron, A.R., Frith, J.E., Gomez, G.A., Yap, A.S., Cooper-White, J.J., 2014. The effect of time-dependent deformation of viscoelastic hydrogels on myogenic induction and Rac1 activity in mesenchymal stem cells. Biomaterials 35, 1857–1868.
Cantini, M., Donnelly, H., Dalby, M.J., Salmeron-Sanchez, M., 2020. The plot thickens: The emerging role of matrix viscosity in cell mechanotransduction. Adv. Healthcare Mater. 9, 1901259.
Cazzell, S.A., Duncan, B., Kingsborough, R., Holten-Andersen, N., 2021. Demonstration of environmentally stable, broadband energy dissipation via multiple metal cross-linked glycerol gels. Adv. Funct. Mater. 31, 2009118.
Charrier, E.E., Pogoda, K., Wells, R.G., Janmey, P.A., 2018. Control of cell morphology and differentiation by substrates with independently tunable elasticity and viscous dissipation. Nat. Commun. 9 (449).
Chaudhuri, O., 2017. Viscoelastic hydrogels for 3D cell culture. Biomater. Sci. 5, 1480–1490.
Chaudhuri, O., Cooper-White, J., Janmey, P.A., Mooney, D.J., Shenoy, V.B., 2020. Effects of extracellular matrix viscoelasticity on cellular behaviour. Nature 584, 535–546.
Chaudhuri, O., Gu, L., Darnell, M., Klumpers, D., Bencherif, S.A., Weaver, J.C., Huebsch, N., Mooney, D.J., 2015. Substrate stress relaxation regulates cell spreading. Nat. Commun. 6 (6365).
Chaudhuri, O., Gu, L., Klumpers, D., Darnell, M., Bencherif, S.A., Weaver, J.C., Huebsch, N., Lee, H.-P., Lippens, E., Duda, G.N., Mooney, D.J., 2016. Hydrogels with tunable stress relaxation regulate stem cell fate and activity. Nat. Mater. 15, 326–334.
Chen, H., Zhang, J., Yu, W., Cao, J., Cao, Z., Tan, Y., 2021. Control viscoelasticity of polymer networks with crosslinks of superposed fast and slow dynamics. Angew. Chem. Int. Ed. 60, 22332–22338.
De Alwis Watuthanthrige, N., Chakma, P., Konkolewicz, D., 2021. Designing dynamic materials from dynamic bonds to macromolecular architecture. Trends Chem. 3, 231–247.
Derrida, B., 1980. Random-energy model: Limit of a family of disordered models. Phys. Rev. Lett. 45, 79–92.
Dey, K., Agnelli, S., Sartore, L., 2019. Dynamic freedom: Substrate stress relaxation stimulates cell responses. Biomater. Sci. 7, 836–842.
Drozdov, A.D., 1997. A constitutive model for nonlinear viscoelastic media. Int. J. Solids Struct. 34, 2685–2707.
Drozdov, A.D., 2014. Self-oscillations of hydrogels driven by chemical reactions. Int. J. Appl. Mech. 6, 1450023.
Drozdov, A.D., Christiansen, J. de C., 2013. Stress–strain relations for hydrogels under multiaxial deformation. Int. J. Solids Struct. 50, 3570–3585.
Drozdov, A.D., Christiansen, J. de C., 2018. Time-dependent response of hydrogels under multiaxial deformation accompanied by swelling. Acta Mech. 229, 5067–5092.
Drozdov, A.D., deClavill Christiansen, J., 2018a. Double-network gels with dynamic bonds under multi-cycle deformation. J. Mech. Behav. Biomed. Mater. 88, 58–68.
Drozdov, A.D., deClavill Christiansen, J., 2018b. Nanocomposite gels with permanent and transient junctions under cyclic loading. Macromolecules 51, 1462–1473.
Drozdov, A.D., deClavill Christiansen, J., 2021. Structure–property relations in linear viscoelasticity of supramolecular hydrogels. RSC Adv. 11, 16860–16880.
Drozdov, A.D., Klitkou, R., Christiansen, J. de C, 2013. Cyclic viscoplasticity of semicrystalline polymers with finite deformations. Mech. Mater. 56, 53–64.
Elosegui-Artola, A., 2021. The extracellular matrix viscoelasticity as a regulator of cell and tissue dynamics. Curr. Opin. Cell Biol. 72, 10–18.
Filippidi, E., Cristiani, T.R., Eisenbach, J.H., Israelachvili, J.N., Ahn, B.K., Valentine, M.T., 2017. Toughening elastomers using mussel-inspired iron-catechol complexes. Science 358, 502–505.
Fullenkamp, D.E., Barrett, D.G., Miller, D.R., Kurutz, J.W., Messersmith, P.B., 2014. Ph-dependent cross-linking of catechols through oxidation via $Fe^{3+}$ and potential implications for mussel adhesion. RSC Adv. 4, 25127–25134.
Gong, Z., Szczesny, S.E., Caliari, S.R., Charrier, E.E., Chaudhuri, O., Cao, X., Lin, Y., Mauck, R.L., Janmey, P.A., Burdick, J.A., Shenoy, V.B., 2018. Matching material and cellular timescales maximizes cell spreading on viscoelastic substrates. Proc. Nat. Acad. Sci. U.S.A 115, E2686–E2695.
Green, M.S., Tobolsky, A.V., 1946. A new approach to the theory of relaxing polymeric media. J. Chem. Phys. 14, 80–92.
Grolma, J.M., Weinand, P., Moone, D.J., 2020. Extracellular matrix plasticity as a driver of cell spreading. Proc. Nat. Acad. Sci. U.S.A 117, 25999–26007.
Guilak, F., Cohen, D.M., Estes, B.T., Gimble, J.M., Liedtke, W., Chen, C.S., 2009. Control of stem cell fate by physical interactions with the extracellular matrix. Cell Stem. Cell 5, 17–26.
Guo, Q., Long, R., 2020. Mechanics of polymer networks with dynamic bonds. Adv. Polym. Sci. 285, 127–164.
Hammer, L., Van Zee, N.J., Nicolay, R., 2021. Dually crosslinked polymer networks incorporating dynamic covalent bonds. Polymers 13 (396).
Han, B., Ma, T., Vergara, J.H., Palmese, G.R., Yin, J., Lee, D., Han, L., 2017. Non-additive impacts of covalent cross-linking on the viscoelastic nanomechanics of ionic polyelectrolyte complexes. RSC Adv. 7, 53334–53345.
Holten-Andersen, N., Harrington, M.J., Birkedal, H., Lee, B.P., Messersmith, P.B., Lee, K.Y.C., Waite, J.H., 2011. pH-induced metal-ligand cross-links inspired by mussel yield self-healing polymer networks with near-covalent elastic moduli. Proc. Nat. Acad. Sci. USA 108, 2651–2655.
Holten-Andersen, N., Jaishankar, A., Harrington, M.J., Fullenkamp, D.E., DiMarco, G., He, L., McKinley, G.H., Messersmith, P.B., Lee, K.Y.C., 2014. Metal-coordination: Using one of nature's tricks to control soft material mechanics. J. Mater. Chem. B 2, 2467–2472.
Janmey, P.A., Fletcher, D.A., Reinhart-King, C.A., 2020. Stiffness sensing by cells. Physiol. Rev. 100, 695–724.
Javadi, M.H., Darijani, H., Niknafs, M., 2021. Constitutive modeling of visco-hyperelastic behavior of double-network hydrogels using long-term memory theory. J. Appl. Polym. Sci. 138 (49894).
Jia, Y., Wang, Y., Niu, L., Zhang, H., Tian, J., Gao, D., Zhang, X., Lu, T.J., Qian, J., Huang, G., Xu, F., 2021. The plasticity of nanofibrous matrix regulates fibroblast activation in fibrosis. Adv. Healthcare Mater. 10, 2001856.

Jiang, Z., Bhaskaran, A., Aitken, H.M., Shackleford, I.C.G., Connal, L.A., 2019. Using synergistic multiple dynamic bonds to construct polymers with engineered properties. Macromol. Rapid Commun. 40, 1900038.
Jing, Y., Yang, B., Yuan, W., Han, S., Song, L., Ye, M., Zhang, Z.-Y., Bian, L., 2021. Dynamic cell-adaptable hydrogels with a moderate level of elasticity promote 3D development of encapsulated cells. Appl. Mater. Today 22, 100892.
Khiem, V.N., Mai, T.-T., Urayama, K., Gong, J.P., Itskov, M., 2019. A multiaxial theory of double network hydrogels. Macromolecules 52, 5937–5947.
Kshitiz Park, J.S., Kim, P., Helen, W., Engler, A.J., Levchenko, A., Kim, D.-H., 2012. Control of stem cell fate and function by engineering physical microenvironments. Integr. Biol. 4, 1008–1018.
Lei, J., Li, Z., Xu, S., Liu, Z., 2021. Recent advances of hydrogel network models for studies on mechanical behaviors. Acta Mech. Sin. 37, 367–386.
Levalley, P.J., Kloxin, A.M., 2019. Chemical approaches to dynamically modulate the properties of synthetic matrices. ACS Macro. Lett. 8, 7–16.
Li, Q., Barrett, D.G., Messersmith, P.B., Holten-Andersen, N., 2016. Controlling hydrogel mechanics via bio-inspired polymer-nanoparticle bond dynamics. ACS Nano 2016 10, 1317–1324.
Lin, J., Zheng, S.Y., Xiao, R., Yin, J., Wu, Z.L., Zheng, Q., Qian, J., 2020. Constitutive behaviors of tough physical hydrogels with dynamic metal-coordinated bonds. J. Mech. Phys. Solids 139, 103935.
Liu, J., Tan, C.S.Y., Yu, Z., Li, N., Abell, C., Scherman, O.A., 2017. Tough supramolecular polymer networks with extreme stretchability and fast room-temperature self-healing. Adv. Mater. 29, 1605325.
Liu, A., Wu, K., Chen, S., Wu, C., Gao, D., Chen, L., Wei, D., Luo, H., Sun, J., Fan, H., 2020. Tunable fast relaxation in imine-based nanofibrillar hydrogels stimulates cell response through TRPV4 activation. Biomacromolecules 21, 3745–3755.
Liu, Y., Zhang, H., Zheng, Y., 2016. A micromechanically based constitutive model for the inelastic and swelling behaviors in double network hydrogels. J. Appl. Mech. Trans. ASME 83, 021008.
Loebel, C., Ayoub, A., Galarraga, J.H., Kossover, O., Simaan-Yameen, H., Seliktar, D., Burdick, J.A., 2019. Tailoring supramolecular guest-host hydrogel viscoelasticity with covalent fibrinogen double networks. J. Mater. Chem. B 7, 1753–1760.
Lou, J., Stowers, R., Nam, S., Xia, Y., Chaudhuri, O., 2018. Stress relaxing hyaluronic acid-collagen hydrogels promote cell spreading, fiber remodeling, and focal adhesion formation in 3D cell culture. Biomaterials 154, 213–222.
Lu, H., Wang, X., Shi, X., Yu, K., Fu, Y.Q., 2018. A phenomenological model for dynamic response of double-network hydrogel composite undergoing transient transition. Composites B 151, 148–153.
Lv, H., Li, L., Sun, M., Zhang, Y., Chen, L., Rong, Y., Li, Y., 2015. Mechanism of regulation of stem cell differentiation by matrix stiffness. Stem Cell Res. Ther. 6 (103).
Ma, Y., Han, T., Yang, Q., Wang, J., Feng, B., Jia, Y., Wei, Z., Xu, F., 2021. Viscoelastic cell microenvironment: Hydrogel-based strategy for recapitulating dynamic ECM mechanics. Adv. Funct. Mater. 31, 2100848.
Mao, T., He, Y., Gu, Y., Yang, Y., Yu, Y., Wang, X., Ding, J., 2021. Critical frequency and critical stretching rate for reorientation of cells on a cyclically stretched polymer in a microfluidic chip. ACS Appl. Mater. Interfaces 13, 13934–13948.
Mao, Y., Lin, S., Zhao, X., Anand, L., 2017. A large deformation viscoelastic model for double-network hydrogels. J. Mech. Phys. Solids 100, 103–130.
Matellan, C., del Rio Hernandez, A.E., 2019. Engineering the cellular mechanical microenvironment – From bulk mechanics to the nanoscale. J. Cell Sci. 132, jcs229013.
Mundhara, N., Yadav, S., Shirke, P.U., Panda, D., Majumder, A., 2021. Substrate loss modulus promotes the differentiation of SHSY-5Y neuroblastoma cells. Materialia 15, 100968.
Nam, S., Lee, J., Brownfield, D.G., Chaudhuri, O., 2016. Viscoplasticity enables mechanical remodeling of matrix by cells. Biophys. J. 111, 2296–2308.
Nam, S., Stowers, R., Lou, J., Xia, Y., Chaudhuri, O., 2019. Varying PEG density to control stress relaxation in alginate-PEG hydrogels for 3D cell culture studies. Biomaterials 200, 15–24.
Nguyen, H.D., Sun, X., Yokota, H., Lin, C.-C., 2021. Probing osteocyte functions in gelatin hydrogels with tunable viscoelasticity. Biomacromolecules 22, 1115–1126.
Picchioni, F., Muljana, H., 2018. Hydrogels based on dynamic covalent and non covalent bonds: A chemistry perspective. Gels 4 (21).
Ren, P., Wang, F., Bernaerts, K.V., Fu, Y., Hu, W., Zhou, N., Dai, J., Liang, M., Zhang, T., 2020. Self-assembled supramolecular hybrid hydrogels based on host-guest interaction: Formation and application in 3D cell culture. ACS Appl. Bio. Mater. 3, 6768–6778.
Richardson, B.M., Walker, C.J., Macdougall, L.J., Hoye, J.W., Randolph, M.A., Bryant, S.J., Anseth, K.S., 2020. Viscoelasticity of hydrazone crosslinked poly(ethylene glycol) hydrogels directs chondrocyte morphology during mechanical deformation. Biomater. Sci. 8, 3804–3811.
Richardson, B.M., Walker, C.J., Maples, M.M., Randolph, M.A., Bryant, S.J., Anseth, K.S., 2021. Mechanobiological interactions between dynamic compressive loading and viscoelasticity on chondrocytes in hydrazone covalent adaptable networks for cartilage tissue engineering. Adv. Healthcare Mater. 10, 2002030.
Richardson, B.M., Wilcox, D.G., Randolph, M.A., Anseth, K.S., 2019. Hydrazone covalent adaptable networks modulate extracellular matrix deposition for cartilage tissue engineering. Acta BioMater. 83, 71–82.
Rizwan, M., Baker, A.E.G., Shoichet, M.S., 2021. Designing hydrogels for 3D cell culture using dynamic covalent crosslinking. Adv. Healthcare Mater. 10, 2100234.
Rodell, C.B., Dusaj, N.N., Highley, C.B., Burdick, J.A., 2016. Injectable and cytocompatible tough double-network hydrogels through tandem supramolecular and covalent crosslinking. Adv. Mater. 28, 8419–8424.
Rosales, A.M., Anseth, K.S., 2016. The design of reversible hydrogels to capture extracellular matrix dynamics. Nat. Rev. Mater. 1 (15012).
Sacco, P., Baj, G., Asaro, F., Marsich, E., Donati, I., 2020. Substrate dissipation energy regulates cell adhesion and spreading. Adv. Funct. Mater. 30, 2001977.
Tanaka, F., Edwards, S.F., 1992. Viscoelastic properties of physically cross-linked networks, transient network theory. Macromolecules 1992 25, 1516–1523.
Tang, S., Richardson, B.M., Anseth, K.S., 2021. Dynamic covalent hydrogels as biomaterials to mimic the viscoelasticity of soft tissues. Progr. Mater. Sci. 120, 100738.
Tang, X., Wang, B., Eristoff, S., Zhang, H., Bettinger, C.J., 2020. Dynamic contributions to the bulk mechanical properties of self-assembled polymer networks with reconfigurable bonds. Macromol. Rapid Commun. 41, 1900551.
Teng, L., Chen, Y., Jia, Y.-G., Ren, L., 2019. Supramolecular and dynamic covalent hydrogel scaffolds: from gelation chemistry to enhanced cell retention and cartilage regeneration. J. Mater. Chem. B 7, 6705–6736.
Tong, Z., Jin, L., Oliveira, J.M., Reis, R.L., Zhong, Q., Mao, Z., Gao, C., 2021. Adaptable hydrogel with reversible linkages for regenerative medicine: Dynamic mechanical microenvironment for cells. Bioactive Mater. 6, 1375–1387.
Vining, K.H., Mooney, D.J., 2017. Mechanical forces direct stem cell behaviour in development and regeneration. Nat. Rev. Mol. Cell Biol. 18, 728–742.
Vining, K.H., Stafford, A., Mooney, D.J., 2019. Sequential modes of crosslinking tune viscoelasticity of cell-instructive hydrogels. Biomaterials 188, 187–197.
von Krbek, L.K.S., Schalley, C.A., Thordarson, P., 2017. Assessing cooperativity in supramolecular systems. Chem. Soc. Rev. 46, 2622–2637.
Wang, H., Heilshorn, S.C., 2015. Adaptable hydrogel networks with reversible linkages for tissue engineering. Adv. Mater. 27, 3717–3736.
Weng, J., Wang, W., 2020. Dynamic multivalent interactions of intrinsically disordered proteins. Curr. Opin. Struct. Biol. 62, 9–13.
Xia, D., Wang, P., Ji, X., Khashab, N.M., Sessler, J.L., Huang, F., 2020. Functional supramolecular polymeric networks: The marriage of covalent polymers and macrocycle-based host-guest interactions. Chem. Rev. 120, 6070–6123.
Xiang, Y., Zhong, D., Rudykh, S., Zhou, H., Qu, S., Yang, W., 2020. A review of physically based and thermodynamically based constitutive models for soft materials. J. Appl. Mech. Trans. ASME 87, 4047776.
Xiao, R., Mai, T.-T., Urayama, K., Gong, J.P., Qu, S., 2021. Micromechanical modeling of the multi-axial deformation behavior in double network hydrogels. Int. J. Plast. 137, 102901.
Yang, Z., Kou, S., Wei, X., Zhang, F., Li, F., Wang, X.-W., Lin, Y., Wan, C., Zhang, W.-B., Sun, F., 2018. Genetically programming stress-relaxation behavior in entirely protein-based molecular networks. ACS Macro Lett. 7, 1468–1474.
Yang, C., Tibbitt, M.W., Basta, L., Anseth, K.S., 2014. Mechanical memory and dosing influence stem cell fate. Nat. Mater. 13, 645–652.
Yesilyurt, V., Ayoob, A.M., Appel, E.A., Borenstein, J.T., Langer, R., Anderson, D.G., 2017. Mixed reversible covalent crosslink kinetics enable precise, hierarchical mechanical tuning of hydrogel networks. Adv. Mater. 29, 1605947.
Yu, K., Xin, A., Wang, Q., 2018. Mechanics of self-healing polymer networks crosslinked by dynamic bonds. J. Mech. Phys. Solids 121, 409–431.
Zhao, L., Zhang, X., Luo, Q., Hou, C., Xu, J., Liu, J., 2020. Engineering nonmechanical protein-based hydrogels with highly mechanical properties: Comparison with natural muscles. Biomacromolecules 21, 4212–4219.